

# Mesenchymal-epithelial transition regulates initiation of pluripotency exit before gastrulation

Sofiane Hamidi<sup>1</sup>, Yukiko Nakaya<sup>2</sup>, Hiroki Nagai<sup>1,2</sup>, Cantas Alev<sup>2,3</sup>, Takeya Kasukawa<sup>4</sup>, Sapna Chhabra<sup>5</sup>, Ruda Lee<sup>6</sup>, Hitoshi Niwa<sup>7</sup>, Aryeh Warmflash<sup>8</sup>, Tatsuo Shibata<sup>2</sup> and Guojun Sheng<sup>1,2,\*</sup>

## ABSTRACT

The pluripotent epiblast gives rise to all tissues and organs in the adult body. Its differentiation starts at gastrulation, when the epiblast generates mesoderm and endoderm germ layers through epithelial-mesenchymal transition (EMT). Although gastrulation EMT coincides with loss of epiblast pluripotency, pluripotent cells in development and *in vitro* can adopt either mesenchymal or epithelial morphology. The relationship between epiblast cellular morphology and its pluripotency is not well understood. Here, using chicken epiblast and mammalian pluripotency stem cell (PSC) models, we show that PSCs undergo a mesenchymal-epithelial transition (MET) prior to EMT-associated pluripotency loss. Epiblast MET and its subsequent EMT are two distinct processes. The former, a partial MET, is associated with reversible initiation of pluripotency exit, whereas the latter, a full EMT, is associated with complete and irreversible pluripotency loss. We provide evidence that integrin-mediated cell-matrix interaction is a key player in pluripotency exit regulation. We propose that epiblast partial MET is an evolutionarily conserved process among all amniotic vertebrates and that epiblast pluripotency is restricted to an intermediate cellular state residing between the fully mesenchymal and fully epithelial states.

**KEY WORDS:** EMT, Epiblast, MET, Pluripotency

## INTRODUCTION

A human embryo at late blastocyst stage of development contains three cell populations: the CDX2<sup>+</sup> trophectoderm, GATA6<sup>+</sup> primitive endoderm and POU5F1<sup>+</sup> epiblast (Blakeley et al., 2015; Deglincerti et al., 2016a). Among them, the epiblast is the only pluripotent population that will give rise to all cell lineages in an adult body. Implantation takes place soon afterwards and loss of pluripotency coincides with the onset of gastrulation when the epiblast initiates lineage differentiation by generating the three definitive germ layers (ectoderm, mesoderm and endoderm). Between pre-implantation and gastrulation (about 1 week in

human development), the epiblast is considered to be pluripotent throughout. But due to ethical and technical limitations, morphogenesis of the epiblast during this period of human development is poorly understood. Different states of pluripotency maintenance *in vitro* have been hypothesized to correspond to unique sub-stages of pre-gastrulation epiblast morphogenesis, e.g. with the naïve and primed states representing the pre-implantation and post-implantation epiblast, respectively (Nichols and Smith, 2009).

Pluripotency markers (e.g. NANOG and POU5F1) are expressed in both pre- and post-implantation epiblast and in their corresponding states captured *in vitro* in the mouse (Najm et al., 2011). Human epiblast is presumed to behave in a similar way, a concept partially supported by data from prolonged *in vitro* culture of human blastocyst and from histological analysis of rare, post-implantation stage human embryos (Deglincerti et al., 2016a; Luckett, 1975, 1978; Vogler, 1987). However, differences between human and mouse development have long been noted, e.g. in topographic arrangement of the epiblast sheet with respect to the rest of the embryo *in vivo* (Sheng, 2015), and in the properties of the embryonic stem cells (ESCs) and induced pluripotent stem cells (iPSCs) cultured *in vitro* (Schnierch et al., 2010). Furthermore, it is unclear whether epiblast intercellular organization plays any role in regulating its pluripotency in either mouse or human development. Except for germ cells, differentiation into somatic cell lineages (in each of the three germ layers) can be achieved from either the naïve or primed ESCs, suggesting that morphogenetic status of pre-gastrulation epiblast is not a key factor in its pluripotency maintenance *in vitro*. Yet, in all amniote species examined, including the birds and mammals, an epithelialized epiblast is a prerequisite for gastrulation to take place *in vivo* (Sheng, 2015), suggesting that epiblast pluripotency status is causally correlated with its morphogenesis.

Epithelialization of mouse epiblast has been shown to be dependent on cell-extracellular matrix (ECM) interactions. Its polarization is regulated by Integrin-linked kinase activity, known to bridge  $\beta 1/2/3$ -integrin cytoplasmic tail to actin cytoskeleton (Sakai et al., 2003), and by both  $\beta 1$ -integrin and dystroglycan, two main types of transmembrane proteins that mediate epiblast-ECM interaction (Li et al., 2017). Modulating cadherin-mediated epiblast cell-cell interactions, by deleting E-cad or replacing E-cad with N-cad, also had a profound effect on epiblast cell-ECM affinity (Basilicata et al., 2016). Weakening of integrin-mediated cell-ECM interaction led to a reduction in E-cad-mediated cell-cell adhesion strength (Martinez-Rico et al., 2010), indicating that cell-ECM and cell-cell interactions, as well as their crosstalk, are crucially involved in epiblast epithelialization (Mui et al., 2016). These lines of evidence suggest that polarization of the epiblast, including the establishment of apicobasal polarity, epiblast-ECM interaction and the modulation of epiblast adherens junction, is involved in epiblast pluripotency regulation.

<sup>1</sup>International Research Center for Medical Sciences (IRCMS), Kumamoto University, Kumamoto 860-0811, Japan. <sup>2</sup>Center for Biosystems Dynamics Research (BDR), RIKEN, Kobe 650-0047, Japan. <sup>3</sup>Institute for the Advanced Study of Human Biology (ASHBi), Kyoto University, Kyoto 606-8507, Japan. <sup>4</sup>Center for Integrative Medical Sciences, RIKEN, Yokohama 230-0045, Japan. <sup>5</sup>Systems, Synthetic and Physical Biology Graduate Program, Rice University, Houston, TX 77251, USA. <sup>6</sup>International Research Organization for Advanced Science and Technology (IROAST), Kumamoto University, Kumamoto 860-8555, Japan. <sup>7</sup>Department of Pluripotent Stem Cell Biology, Institute of Molecular Embryology and Genetics, Kumamoto University, Kumamoto 860-0811, Japan. <sup>8</sup>Department of Biosciences and Bioengineering, Rice University, Houston, TX 77005, USA.

\*Author for correspondence (sheng@kumamoto-u.ac.jp)

 G.S., 0000-0001-6759-3785

To understand how epiblast morphology regulates its pluripotency, we first investigated whether its epithelialization could be viewed as a mesenchymal-epithelial transition (MET) process, the reverse of epithelial-mesenchymal transition (EMT) (Lamouille et al., 2014). Using a combination of *in vivo* (chicken epiblast) and *in vitro* [human iPSCs (hiPSCs), human ESCs (hESC) and mouse PSCs (mESCs and mEpiSCs)] models, we asked whether epiblast MET played a role in epiblast pluripotency maintenance and, if so, how this could offer us insight into normal pre-gastrulation development of the human embryo. We present data showing that amniote epiblast goes through a partial MET process that is primarily characterized by the segregation of basal and lateral plasma membrane domains of the epiblast and by the deposition of epiblast basement membrane. This partial MET regulates the initiation of pluripotency exit through activation of the integrin-mediated signaling pathway.

## RESULTS

### Avian epiblast undergoes epithelialization and initiates pluripotency exit before the onset of gastrulation

Using the analogy of Waddington's epigenetic landscape of lineage specification (Waddington, 1952), the loss of pluripotency in amniote development is marked by gastrulation, a process in which the epiblast gives rise to the three definitive germ layers (the ectoderm, mesoderm and endoderm). We and others have previously shown that gastrulation in chick embryos, taking place mainly at Hamburger and Hamilton stages (HH) 3 and 4 (about 12–18 h of development after egg laying), requires an epithelial-mesenchymal transition (EMT) process to convert epithelial-shaped epiblast cells into mesenchymal-shaped mesendoderm precursors (Bellairs, 1986; Hay, 1968; Nakaya et al., 2013, 2008). We and others have also reported that gastrulation EMT is associated with the loss of pluripotency markers in the epiblast at ~HH5, when neural ectoderm fate is specified (Laval et al., 2007; Shin et al., 2011). To investigate the dynamic relationship between epiblast EMT and its pluripotency loss, we carried out a transcriptomic analysis of pre- and peri-gastrulation stage chicken embryos (HH1–HH3; 0.5h–14 h of development) (Fig. S1A). Area pellucida (intra-embryonic) epiblast tissues, excluding the forming primitive streak, were collected and used for Affymetrix genechip-based transcriptome analysis (see Materials and Methods). Differential expression analysis (Table S1) showed that 5529 (of 38,535 in total) probe sets had statistically significant cross-stage variations (FDR<0.01), with 2376 exhibiting an increasing trend (Fig. S1B; 0001, 0011 and 0111 clusters) and 2543 a decreasing trend (Fig. S1C; 1000, 1100 and 1110 clusters). Gene ontology analysis revealed an enrichment of biological processes associated with epithelial morphogenesis from stage HH2 onwards (0001 cluster) (Table S2). Conversely, a large number of early HH1-specific genes (cluster 1000) were associated with RNA and nucleic acid binding, modification and metabolism (Table S2), likely reflecting their involvement in pluripotent maintenance at ovipositional stages as previously reported (Mak et al., 2015). This was supported by the analysis of candidate genes known to be involved in pluripotency regulation (e.g. NANOG, SOX3, FLF3, OTX2, TCF7L2, MYC, DNMT3 and LIN28) and epithelial morphogenesis (e.g. COL4 genes, SDC genes) (Fig. S1D; Table S1). Further confirmation came from re-analysis of our recently published developmental promoterome datasets (Lizio et al., 2017). Although whole embryos, including both the area pellucida and area opaca, were used in that paper, a general decrease in promoter activities of pluripotency-related genes and increase in those of epithelial genes

were observed prominently in the first day of chick development (HH1–HH7) (Fig. S2). Taken together, these data suggested that, in addition to the well-known phase of pluripotency loss associated with gastrulation EMT and taking place at HH3–HH5, a decrease in pluripotency marker expression is seen much earlier from late HH1 and is possibly associated with an increase in epithelial-associated features of the epiblast.

### Avian epiblast is characterized by a partial mesenchymal-epithelial transition (MET) at late HH1 followed by a full EMT during gastrulation at HH3

To better characterize this epithelialization process, we analyzed HH1 embryos with epithelial polarity markers (Fig. 1). We compared embryos from freshly laid eggs, at Eyal-Giladi and Kochav (Eyal-Giladi and Kochav, 1976; Kochav et al., 1980) (EGK) X/XI sub-stages of HH1 (referred to as early HH1 in this work), with embryos from eggs incubated for 6 h, at EGK-XIII/XIV sub-stages of HH1 (referred to as late HH1). At late HH1, epiblast polarity had already been clearly established, as evidenced by the presence of a continuous layer of basement membrane (Laminin and Agrin; Fig. 1A), presence of apical membrane domain (aPKC; Fig. 1G,H) and apical tight junctions (ZO-1; Fig. 1E,F), segregation of basal and lateral membrane domains marked by the lateral localization of E-cad (Fig. 1B), and basal enrichment of  $\beta$ 1 integrin and dystroglycan (Fig. 1C,D), and enrichment of Golgi apparatus (GM130; Fig. 1I,J) and acetylated tubulin (Fig. 1K,L) in the cytoplasm apical to the nucleus. Interestingly, all these markers were also expressed at early HH1, but at lower levels and/or in a much less organized fashion (Fig. 1; 0 h). Laminin and agrin at early HH1 were expressed spottily under a small percentage of epiblast cells (Fig. 1A) and E-cad marked both lateral and basal regions of an epiblast cell (Fig. 1B). Both ZO-1 and aPKC exhibited apically compartmentalized uneven distribution at early HH1 (Fig. 1E,G). Taken together, these data suggested that, at early HH1, epiblast cells exhibit weak epithelial features and they become fully epithelialized within ~6 h of development when the embryo reaches late HH1 (Fig. S3), which is ~6 h before the onset of gastrulation at HH3. This transition from a weakly polarized organization to a fully epithelial organization can be viewed as epithelioid-to-epithelial transition (referred to as a partial mesenchymal-epithelial transition in this work; partial MET). We then used laminin expression as an indicator of the extent of this partial MET and NANOG protein expression as an indicator of epiblast pluripotency, and investigated their relative and dynamic changes from HH1 to HH3 (Fig. S4A–D). Before full epithelialization, a small increase in NANOG levels was observed from early HH1 to late HH1 (Fig. S4A,B). This likely corresponded to the final step of epiblast-hypoblast sorting through polygression, as previously reported (Harrisson et al., 1991; Stern and Downs, 2012; Weinberger and Brick, 1982), which in the mouse is associated with a loss of GATA6 and increase of NANOG (Mathew et al., 2019). After full epithelialization, NANOG levels in epiblast cells decreased steadily from late HH1 (Fig. S4B) to late HH2 (Fig. S4C) and late HH3 (Fig. S4D). As shown previously (Shin et al., 2011), after gastrulation EMT, mesendoderm cells lost their pluripotency marker expression completely (Fig. S4D).

### Undifferentiated hiPSCs exhibit a size-dependent shift in macroscopic patterns of pluripotency gene expression

Similar to the avian epiblast, mammalian pluripotent cells appear also to undergo an epithelialization process in their morphogenesis, i.e. from non-epithelial epiblast precursors in the inner cell mass to

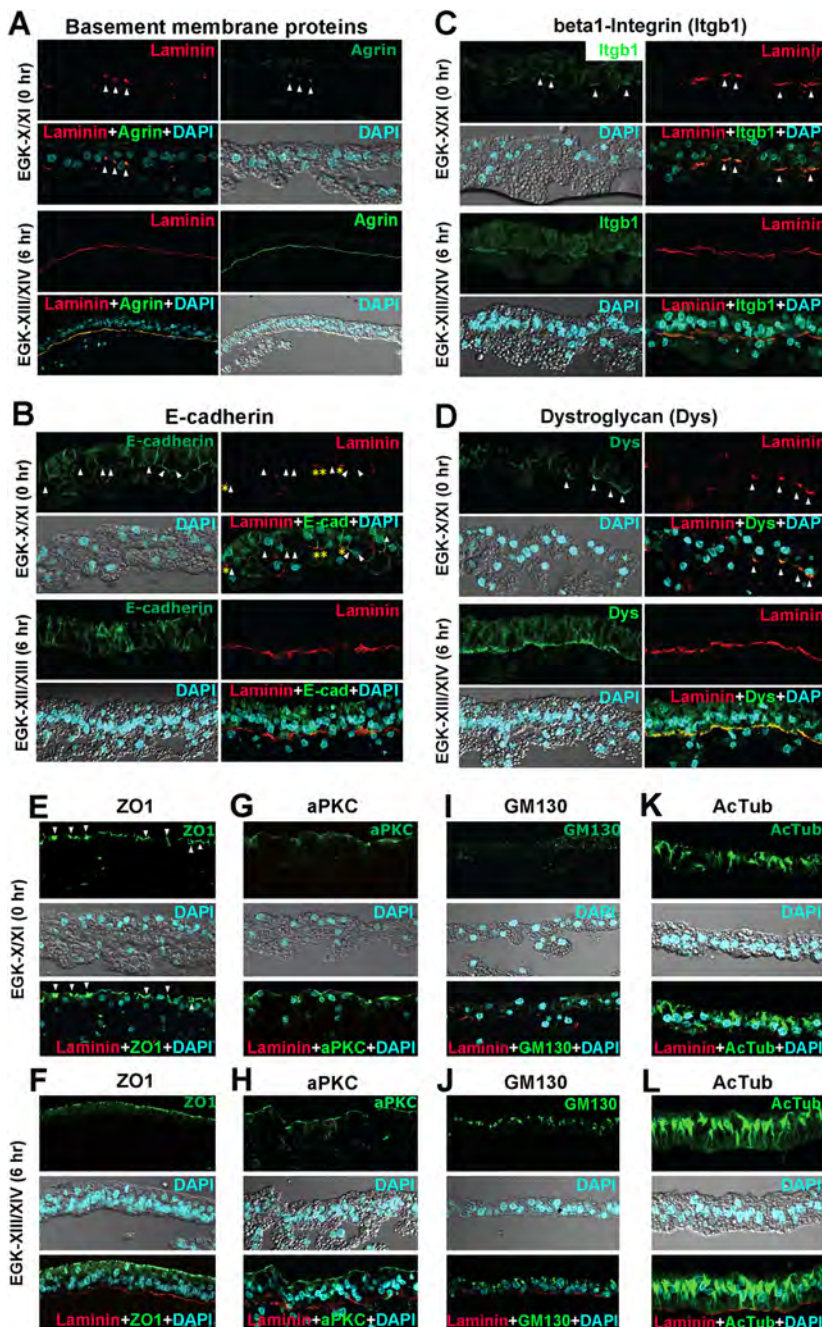


**Fig. 1. Immunofluorescence staining of HH1 chicken epiblast with epithelial markers.** (A) Laminin (red), agrin (green) and DAPI (cyan) staining of unincubated (EGK-X/XI) and 6 h incubated (EGK-XIII/XIV) embryos. At EGK-X/XI, basement membrane (BM) is absent or very immature (arrowheads). At EGK-XIII/XIV, BM is mature. (B) Laminin (red), E-cad (green) and DAPI (cyan) staining of unincubated (EGK-X/XI) and 6 h incubated (EGK-XIII/XIV) embryos. At EGK-X/XI, distinction between basal and lateral membrane domains is not clear and E-cad is expressed in both domains (arrowheads). In epiblast cells with BM deposition, basal E-cad localization is suppressed (asterisks). Epiblast cell height is uneven. At EGK-XIII/XIV, most of epiblast cells have BM underneath them and have laterally restricted E-cad expression. (C) Laminin (red),  $\beta$ 1-integrin (green) and DAPI (cyan) staining of unincubated (EGK-X/XI) and 6 h incubated (EGK-XIII/XIV) embryos. (D) Laminin (red), dystroglycan (green) and DAPI (cyan) staining of unincubated (EGK-X/XI) and 6 h incubated (EGK-XIII/XIV) embryos. (E, G, I, K) Unincubated embryo (EGK-X/XI) stained for ZO-1 (E), aPKC (G), GM130 (I) and acetylated tubulin (K). (F, H, J, L) Embryos incubated for 6 h (EGK-XIII/XIV) stained for ZO-1 (F), aPKC (H), GM130 (J) and acetylated tubulin (L). All sections were co-stained for laminin (red) and DAPI (cyan).

an epithelial epiblast surrounding a proamniotic cavity before gastrulation (Bedzhov and Zernicka-Goetz, 2014). We hypothesized that such a partial MET, similar to the case in the chick, is crucial for mammalian pluripotency regulation, possibly marking a so far undescribed initiation checkpoint of pluripotency exit. To test this hypothesis, we used cultured human induced pluripotent stem cells (hiPSCs; 201B7 line) (Takahashi et al., 2007) as a surrogate for the human epiblast tissue. hiPSCs can be kept in a pluripotent state under maintenance conditions and can give rise to cell lineages in all three germ layers upon receiving differentiation cues. Single-cell level heterogeneity in pluripotency marker expression has been reported for hiPSCs cultured under maintenance conditions (Cahan and Daley, 2013; Chambers et al., 2007; Narsinh et al., 2011).

We first asked whether a similar heterogeneity could be observed at the macroscopic level. To reveal dynamic changes in gene

expression, we used the RNA *in situ* hybridization method and analyzed expression patterns of key pluripotency regulatory genes *POU5F1*, *NANOG* and *LEF1* in hiPSCs (Materials and Methods; Fig. 2A). For all genes, we observed two types of hiPSC colonies (Fig. 2A): one with a ubiquitous and centrally high expression [referred to as center (+) colonies in this work] (Fig. 2A, top panels; Fig. 2C); the other with a pericentrally high, but centrally low or negative expression [referred to as center (–) colonies in this work] (Fig. 2A, bottom panels; Fig. 2C). Statistical analysis revealed that center (+) colonies were generally smaller (with a colony radius of  $304.6 \pm 12.3 \mu\text{m}$  and  $n=53$  for *POU5F1*) than the center (–) colonies (with a colony radius of  $553.7 \pm 27.6 \mu\text{m}$  and  $n=30$  for *POU5F1*) (Fig. 2A,B). Similarly, a strong size-pattern correlation was observed for other genes (Fig. 2B). To understand this dynamic shift better, we divided each *POU5F1*-positive colony into sub-

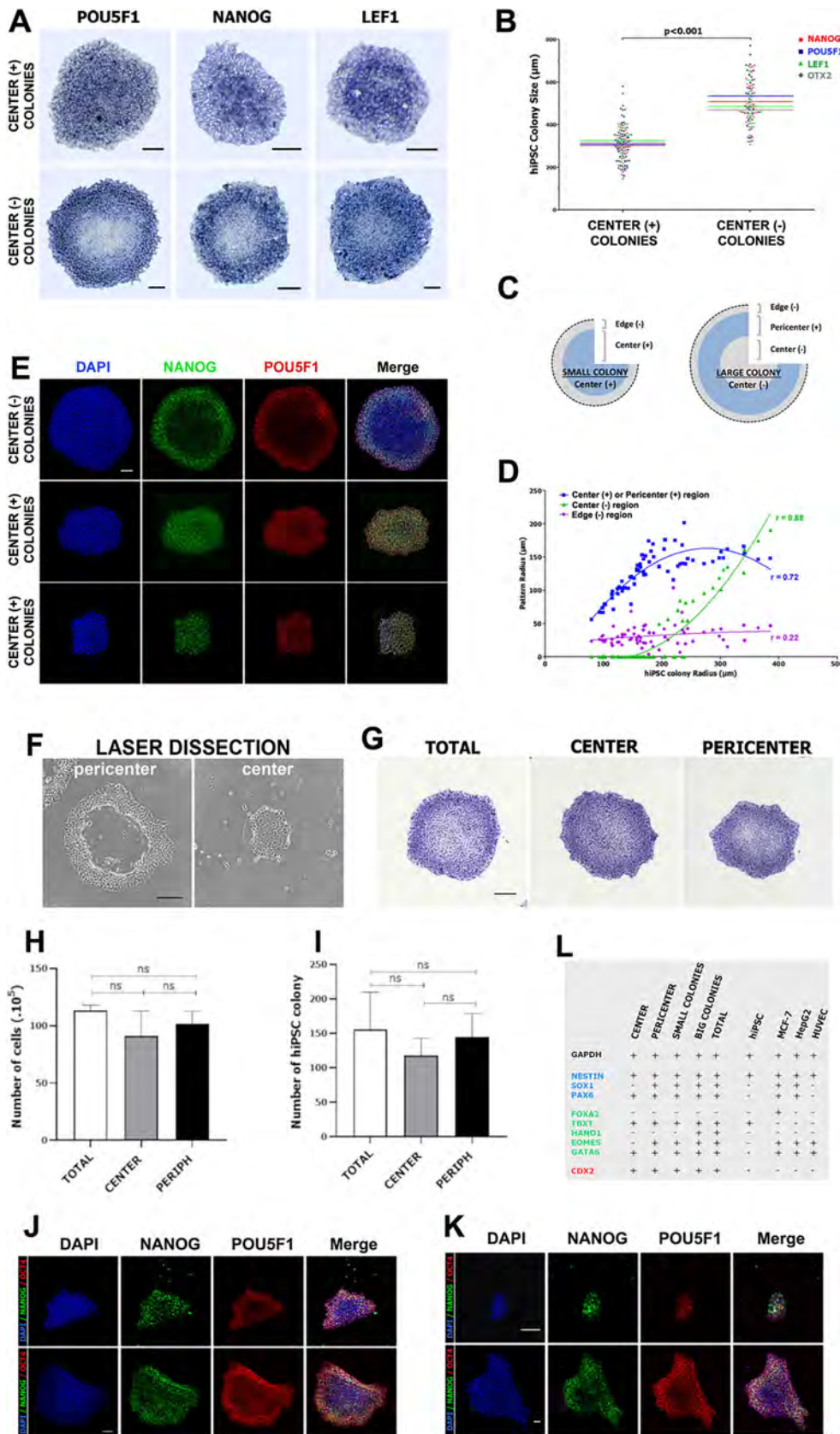


**Fig. 2. Undifferentiated hiPSCs exhibit dynamic patterning of pluripotency gene expression without pluripotency loss.** (A) RNA *in situ* hybridization analysis of POU5F1, NANOG and LEF1 in hiPSC colonies at day 6 of culture, revealing two types of hiPSC colony organization: central (+) or central (-). Details of each type are shown in C. (B) Correlation of colony size (diameter in µm) and colony type [center (-) or center (+)] for NANOG, POU5F1 and LEF1 and OTX2. (C) Schematic organization of the two colony types. Small colonies (~300 µm in diameter) are center (+) and large colonies (~500 µm in diameter) are center (-). In each case, there is an 'edge' sub-territory that has low RNA expression associated with flattened cell morphology. This edge (-) sub-territory defines the boundary of colony and is not studied in detail in this work. (D) Correlation analysis between the width (pattern radius) of those three sub-territories and hiPSC colony radius. Pearson correlation coefficient (r) is provided. Lines correspond to a nonlinear polynomial order 2 (quadratic) regression curve based on the plotted points. (E) Confocal images of NANOG and POU5F1 protein expression in hiPSC colonies of increasing sizes (bottom to top). (F) Laser-assisted microdissection of center and pericenter cells in patterned large hiPSC colonies. (G) POU5F1 RNA. After re-culture (by passaging) of microdissected cells, both center-derived and pericenter-derived cells were able to re-form size-dependent colony patterning, with no clear differences between them or with whole-colony re-cultures. (H,I) Statistical analysis of cell number and colony number after re-culture. No significant difference, either in number of post-culture cells (H) or in the number of colonies formed (I), could be seen between total-, center- and pericenter-derived cells. (J,K) After laser microdissection, the remaining cells in the colony, either as center cells (K) or as half a colony (J), could continue colony growth and re-form a patterned colony. (L) Without re-culture, differentiation potentials of center cells favored the ectoderm lineage. Microdissected hiPSCs were collected, aggregated and induced to differentiate (see Materials and Methods), followed by expression analysis of germ layer-specific markers. Center-derived hiPSCs had a reduced ability to form mesoderm lineages. Scale bars: 100 µm.

territories, as schematized in Fig. 2C, and analyzed their correlation with the colony size (Fig. 2D). The center (-) territory was strongly correlated with the overall colony size (Fig. 2D, green) (Pearson

correlation coefficient  $r=0.88$ ; two-tailed  $t$ -test  $P<0.001$ ). A clear correlation ( $r=0.72$ ,  $P<0.001$ ) was also seen between the colony size and the width of POU5F1-positive territories [center (+) region in

small colonies and pericenter (+) region in big colonies as shown in Fig. 2D], with an initial positive association (up to 450  $\mu\text{m}$  in colony size) and a gradual shift to a steady state width of  $\sim 150 \mu\text{m}$  (Fig. 2D blue). On the contrary, no correlation between the colony size and the edge territory was observed ( $r=0.22$ ,  $P=ns$ ) (Fig. 2C; Fig. 2D purple). This overall dichotomy in expression patterns was further supported by POU5F1 and NANOG immunofluorescence analysis (Fig. 2E). Taken together, these data suggested that hiPSCs cultured under pluripotency maintenance conditions undergo a macroscopically predictable change in pluripotency gene expression during their expansion from a few cells to a colony of hundreds of cells before passaging.

### Reduction in pluripotency gene expression in hiPSC colonies is a reversible process with no loss of pluripotency after re-culture

To test whether reduced pluripotency gene expression in center (–) colonies was indicative of an irreversible pluripotent loss, we isolated center and pericenter cells through laser microdissection (Fig. 2F) (see Materials and Methods). Isolated cells were treated with ROCK inhibitor Y-27632 for 2 h before dissociation and re-culture in normal maintenance media. Both center-derived and pericenter-derived hiPSCs were capable of growth and re-formation of the originally patterned colonies (Fig. 2G), with no significant difference in either the total cell number (Fig. 2H) or colony number (Fig. 2I) after re-culture. When large colonies were micro-dissected to remove pericenter cells, leaving only center (–) cells (Fig. 2K, top), such colonies were able to re-form large and patterned colonies after continuation of the culture without passaging (Fig. 2K, bottom). Similarly, bisected colonies (with half of the colony removed) were also able to re-establish patterning after continuation of the culture (Fig. 2J). These data showed that, despite having much reduced levels of pluripotency gene expression, hiPSCs located in the colony center still retained their pluripotency and that such pluripotency could be manifested after dissociation or disruption of original colony organization. However, center and pericenter cells did exhibit biased differentiation capability (Fig. 2L). When we collected micro-dissected center and pericenter cells for direct differentiation (see Materials and Methods), pericenter cells had the full capability (compared with non-dissected hiPSC colonies) to differentiate into the three germ layers, whereas center cells had reduced capability to differentiate into mesoderm fate (Fig. 2L).

### The decrease in hiPSC pluripotency is correlated with an increase in its ‘epithelialness’

Full pluripotency loss takes place during gastrulation EMT. Our data on the chicken epiblast suggested that an important landmark of pluripotency exit is the transition from a non-epithelial epiblast to an epithelial epiblast (i.e. epiblast MET rather than EMT). We asked whether this macroscopic shift in pluripotency gene expression in hiPSC colonies described above was correlated with changes in their epithelial status. Close observation indicated that, in small colonies, cells in the center were loosely packed (Fig. 3A,C). In large colonies, only colony-pericenter cells showed similar loose packing, whereas colony-center cells were arranged tightly (Fig. 3B,D). This was supported by histological sections of hiPSC colonies cultured on polycarbonate membrane (Fig. 3E, top and middle panels). A unilaminar (single-cell layered) organization of hiPSCs, regardless of colony size, was also evident from histology and confocal analyses (Fig. 3E,H-K). Flattened cells at the colony edge (Fig. 3A-E) were POU5F1 RNA-low cells [labeled as edge (–) in Fig. 2C]. Those cells defined colony boundary, were involved in colony size expansion,

and were not studied further in this work. Intercellular space seen in loosely packed cells (center cells in small colonies and pericenter cells in large colonies) (Fig. 3A-E) was restricted to the basal side because little intercellular space was observed at the apical side of either tightly packed cells in the center (Fig. 3F, left) or loosely packed cells in the pericenter (Fig. 3F, right). Similar to the temporal progression of epithelial maturation described in the avian epiblast (Fig. 1), a spatial progression of epithelial maturation was seen in hiPSCs (Fig. 3G-K). Both ZO-1 (tight junction marker) (Fig. 3G,H) and E-cad (adherens junction marker) (Fig. 3G,I) were expressed in both center (tightly packed) and pericenter (loosely packed) cells. However, ZO-1 and E-cad were diffusely localized in pericenter cells (Fig. 3H,I), characteristic of an immature epithelium (Siliciano and Goodenough, 1988; Woichansky et al., 2016), whereas in center cells, E-cad (Fig. 3I) was localized to the lateral membrane and ZO-1 (Fig. 3H) to the apical junctions, as expected for a mature epithelial organization. The full epithelial nature of center cells was further supported by deposition of basement membrane proteins (HSPG2 in Fig. 3J; LAMA1 in Fig. 3K) under colony center cells, but not pericenter cells. Interestingly, apical membrane marker aPKC did not exhibit prominent difference in either expression level or localization between center and pericenter cells (Fig. 3L), suggesting that the pericenter cells, although not fully epithelial, exhibit partial epithelial characteristics and that these cells will progressively mature into a full epithelium as the colony expands. Collectively, these data show that hiPSCs under pluripotency maintenance culture conditions undergo a partial MET that is correlated with a reduction in their pluripotent gene expression. Taking both chick epiblast and hiPSC data into consideration, we called this phenomenon MET-associated initiation of pluripotency exit, in order to distinguish it from the loss of pluripotency associated with gastrulation EMT.

### Perturbation of MET alters initiation of pluripotency exit

To test whether the association between MET and pluripotency is causal, we used the Rho-kinase inhibitor Y-27632 to perturb the MET process. We have previously shown that the activity of small GTPase RhoA is essential for the maintenance of epithelial status of the epiblast during gastrulation EMT (Nakaya et al., 2008). Y-27632, a potent inhibitor of Rho-associated protein kinases and of RhoA activity, was reported to increase the survival of dissociated hiPSCs without significantly altering their pluripotency status (Watanabe et al., 2007). After 48 h of Y-27632 treatment (20  $\mu\text{M}$ ; from day 4 to day 6 of culture), cells in the center of hiPSC colonies adopted a loosely packed morphology (Fig. 3E, bottom panel) compared with the control (Fig. 3E, middle panel), suggesting that the process of partial MET in the colony center was inhibited. Statistical analysis revealed that Y-27632 also caused a reduction in the height of hiPSCs (Fig. 4A; black control  $r=0.82$   $P<0.001$ , blue Y27632,  $r=0.50$ ,  $P<0.001$ ) and height heterogeneity (measured by max/min cell height ratio; Fig. 4B; black control,  $r=0.81$ ,  $P<0.001$ ; blue, Y27632,  $r=0.20$ , not significant). We then asked whether Y27632 could affect pluripotency exit as described above. After either 24 h (day 5 to 6) or 48 h (day 4 to 6) treatment with Y-27632, iPSC colonies were analyzed for POU5F1 expression. Two types of POU5F1-expressing colonies were observed in both cases (Fig. 4C), similar to the control. A dramatic increase in colony size, however, was observed after both 24 h and 48 h treatment, and in both colony types (Fig. 4D for center-positive colonies and Fig. 4E for center-negative colonies), consistent with the reduction in cell-cell compactness (Fig. 3E) and cell height (Fig. 4A,B). Moreover, in the 24 h treatment group, the relative ratio of center-negative and pericenter-positive territories in

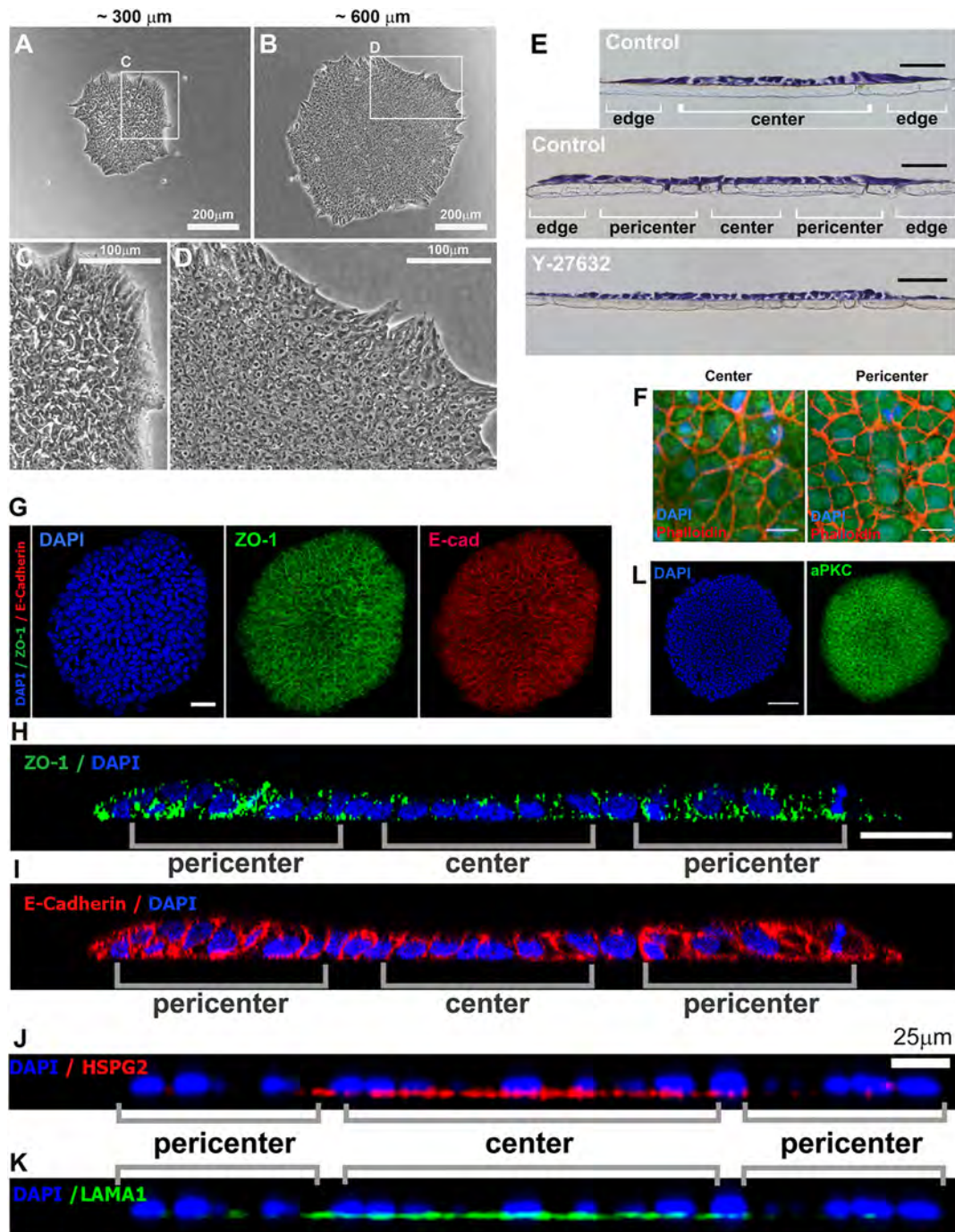


**Fig. 3. Epithelial status of hiPSC colonies.** (A-D) Bright-field views of small (A; magnified view in C) and large (B; magnified view in D) hiPSC colonies, showing loose intercellular organization in small colonies (A,C) and tight intercellular organization in large ones (B,D). Scale bars: 200  $\mu\text{m}$  in A and B; 100  $\mu\text{m}$  in C and D. (E) Histological section of hiPSCs grown on a polycarbonate membrane, supporting the observation in A-D. Top panel, small colony; middle, large colony; bottom, colony treated with ROCK inhibitor Y-27632. Scale bar: 40  $\mu\text{m}$ . (F) Confocal images of the apical side of a large colony, showing its center (left panel) and pericenter (right panel) areas. In both areas, hiPSCs do not show any intercellular gap between cells. (G-K) Representative immunofluorescence images of a hiPSC colony stained for the tight junction marker ZO-1 (colony view in G, z-section view in H), the adherens junction marker E-cad (colony view in G, z-section view in I), the basement membrane markers HSPG2 (z-section view in J) and LAMA1 (z-section view in K), and the apical marker aPKC (colony view in L). aPKC staining is uniform in the colony (L). ZO-1 and E-cad show a stronger, but less localized expression in the colony pericenter. In the colony center, both ZO-1 and E-cad exhibit epithelial-like localized organization, with ZO-1 at the apical junction and E-cad at the lateral membrane. HSPG and laminin deposition are prominent only in the colony center. Scale bars: 20  $\mu\text{m}$  in F; 100  $\mu\text{m}$  in L.

large colonies was changed (Fig. 4C,F), resulting in an increase in the POU5F1-positive pericenter territory at the expense of POU5F1-negative territory (Fig. 4C,F; green, 24 h treated; blue, control). This increase in the POU5F1-positive pericenter territory was correlated

with the increase in the overall colony size ( $r=0.72$ ,  $P<0.001$ ) (Fig. 4F). These observations were further supported by the analysis using POU5F1 and NANOG antibodies (Fig. 4G). In the 48 h treatment group, the size of POU5F1-positive territory became

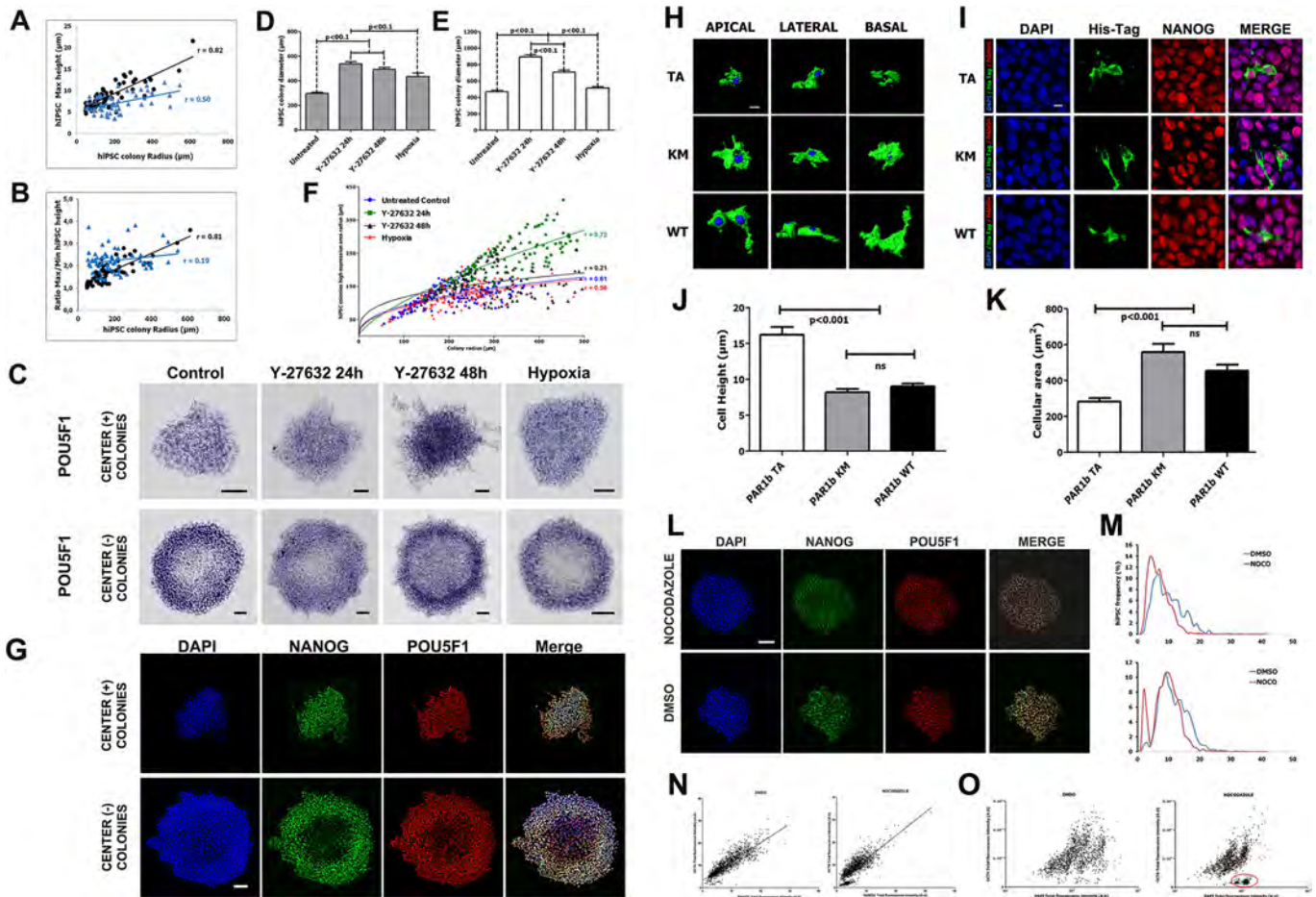


**Fig. 4. Perturbation of MET alters pluripotency gene expression and cell height modulation does not induce pluripotency exit.** (A,B) Correlation plots of the cellular height and the colony radius in each hiPSC colony. Pearson correlation coefficient ( $r$ ) is provided. Lines correspond to the linear regression based on the plotted point. Black, control; blue, Y-27632 treated. (A) Correlation of colony radius with maximum cell height. (B) Correlation of colony radius with the ratio between maximum/minimum cell height. Y-27632 reduces hiPSC max height and disrupts intra-colony height ratio organization and its correlation with colony size. (C-F) RNA *in situ* hybridization analysis of POU5F1 in hiPSC colonies at day 6 of culture in control, Y-27632-treated (24 h and 48 h) and hypoxia-treated (5%  $O_2$  for 6 days) conditions. (C) Representative images of POU5F1 expression after treatment. Scale bars: 100  $\mu$ m. (D,E) Analysis of center (+) (D) and center (-) (E) hiPSC colony diameter in these culture conditions. (F) Correlation analysis between the colony radius and the width of pluripotency gene-expressing areas [center (+) or pericenter (+) sub-territories]. Lines correspond to a logarithmic nonlinear regression curve based on the plotted points. Pearson correlation coefficient ( $r$ ) is indicated. (G) Confocal images of POU5F1 and NANOG protein expression in hiPSC colonies treated with Y-27632 for 24 h. Scale bar: 100  $\mu$ m. (H-K) Analysis of hiPSC morphological changes 48 h after transfection with expression vectors for one of the PAR1b protein mutant forms: PAR1b-TA, -KM or -WT (see Materials and Methods). (H) Representative images of apical (left), lateral (middle) or basal (right) projected 3D reconstruction of hiPSCs, showing that PAR1b-TA significantly increased hiPSC height and decreased apically or basally projected cell areas (quantification in J and K, respectively). Scale bar: 5  $\mu$ m. (I) Co-staining of PAR1b (His-tag) and NANOG, showing that NANOG expression is not altered by PAR1b overexpression. Scale bar: 5  $\mu$ m. (L-O) NANOG and POU5F1 expression after nocodazole treatment. (L) Representative confocal images of NANOG and POU5F1 protein expression after DMSO or nocodazole treatment. Scale bar: 100  $\mu$ m. (M) Distribution analysis of NANOG (top panel) and POU5F1 (bottom panel) expression levels (in arbitrary fluorescence units) for DMSO- (blue) and nocodazole- (red) treated cells, showing a modest decrease in fluorescence intensity after nocodazole treatment. (N,O) Correlation plots between POU5F1 and NANOG (N), and between POU5F1 and DAPI (O) expression levels. Line slope corresponds to the linear regression for those cells. Red outline in O highlights the DAPI-high POU5F1-low population, which is under cell-cycle arrest.

variable and lost any correlation with the colony size ( $r=0.21$ ,  $P<0.05$ ) (Fig. 4C,F), although a mild increase throughout the colony in POU5F1 expression levels was observed for this group (Fig. 4C). To test whether such perturbation of patterning was specific to Y-27632, we cultured hiPSCs for 6 days (the entire duration of culture) under hypoxia (5%  $O_2$ ), which had been reported to promote pluripotency maintenance in ESCs (Forristal et al., 2010; Mathieu et al., 2013). Hypoxia caused a small increase in overall colony size (Fig. 4C-E), but without altering the patterning of the colony (Fig. 4F; compare red and blue lines;  $r=0.56$  and  $r=0.61$ , respectively, with  $P>0.001$  in both conditions). Taken together, these data suggest that Y-27632 treatment disrupted

the partial MET in hiPSC colonies and resulted in a delay in MET-induced pluripotency exit and a mild increase in pluripotency marker expression.

#### Epithelial cell height is not a significant indicator of pluripotency exit

After epithelialization but before gastrulation, the epiblast in both chicken and human embryos undergoes further morphogenetic changes, among which is an increase in cell height. During gastrulation EMT (pluripotency loss), epiblast cells are typically of columnar epithelial morphology. In this study, we observed heterogeneity in hiPSC height (Fig. 4A; black control), although

a simple correlation between cell height and pluripotency level could not be established. To test whether cell height plays an instructive role in pluripotency exit, we used a constitutively active version of human PAR1b (hPAR1b-TA; Materials and Methods) to regulate hiPSC height. PAR1 is a serine-threonine kinase important for cellular polarity establishment and maintenance. hPAR1b-TA (T595A), a non-phosphorylatable version of hPAR1b that renders it 'constitutively active', has been shown to promote basolateral membrane domain at the expense of apical domain and to increase the cell height of MDCK monolayer (Masuda-Hirata et al., 2009). As expected, expression of hPAR1b-TA in hiPSCs (analyzed 48 h after transfection) led to a dramatic increase in cell height (Fig. 4H, lateral view; Fig. 4J, quantification), as well as to a decrease in projected cell surface area (Fig. 4A, apical and basal views; Fig. 4K, quantification). However, co-immunofluorescence analysis of hPAR1b-TA (revealed using an antibody against His-tag) and NANOG showed that no significant change in pluripotency level could be associated with increased cell height (Fig. 4I). Neither wild-type hPAR1b (hPAR1b-WT) nor a kinase-dead mutant of hPAR1b (hPAR1b-KM) had a clear effect on either cell height (Fig. 4H,J,K) or pluripotency marker level (Fig. 4I). These data, together with our observation that, in both chick epiblast (Fig. 1) and hiPSC colonies (Fig. 3), the apical domain marker aPKC was already correctly localized at the immature epithelial stage, suggest that the segregation of apical and basolateral membrane domains is not a key factor in this partial MET or pluripotency exit.

#### Integrin-mediated compartmentalization of lateral and basal domains regulates pluripotency exit

We then asked whether subdivision of the basolateral domain into basal and lateral domains, mediated by dynamic interplay between cell-matrix and cell-cell contacts, could play a role in pluripotency exit. We first tested the effect of nocodazole on pluripotency gene expression. Nocodazole can destabilize microtubule network and lead to basement membrane degradation of chicken epiblast cells during gastrulation EMT at HH3/4 (Nakaya et al., 2011, 2008), potentially erasing the difference between the basal and lateral membrane domains. However, nocodazole was also shown to reduce pluripotency marker expression through an upregulation of TP53 in ESCs (Kallas et al., 2011). Treatment of HH1 embryo with nocodazole (3 h; 10  $\mu$ g/ml) led to disruption of epithelial integrity and to a modest decrease in NANOG protein expression levels (Fig. S4E,F). hiPSCs treated with nocodazole (10  $\mu$ g/ml) for 24 h became detached from the dish. Treatment for 3 h (10  $\mu$ g/ml) caused a mild, but statistically significant, drop in NANOG and POU5F1 expression levels (Fig. 4L; Fig. 4M; red, nocodazole; blue, control;  $n=3$ ). NANOG and POU5F1 intensities showed tight correlation in both control and nocodazole-treated groups (Fig. 4N), except for a small population of mitotically arrested cells (Fig. 4O, right) that had a strongly reduced level of POU5F1 expression (Fig. 4N,O). Taken together, these data suggest that microtubule destabilization has a complex, but not prominent, effect on hiPSC pluripotency exit.

We next tested whether integrin-mediated cell-matrix interaction played a role in pluripotency exit. Both chicken epiblast and hiPSCs expressed  $\beta$ 1 integrin as the major  $\beta$  isoform (Fig. 1C; Fig. 5A; Table S3). The blocking antibody for  $\beta$ 1 integrin (P5D2; Materials and Methods) would block  $\beta$ 1 integrin-mediated cell-matrix interaction, but not the E-cad-mediated cell-cell interaction. Treatment for 24 h with the blocking antibody (1  $\mu$ g/ml) led to complete detachment of hiPSCs, suggesting that it had a potent effect on cell-matrix interactions. Treatment for 2 h with  $\beta$ 1 integrin blocking antibody (1  $\mu$ g/ml) did not cause obvious morphological

abnormality, but resulted in a robust upregulation of POU5F1 expression in all colonies and erased the center (–) territory in large colonies (Fig. 5B), suggesting that integrin-mediated cell-matrix interaction was a key regulator of pluripotency exit. Prolonged treatment (48 h) of hiPSCs with much lower concentrations of  $\beta$ 1-integrin blocking antibody (10 ng/ml and 24 ng/ml), however, resulted in reduction in pluripotency marker expression (Fig. 5C). Interestingly, both concentrations (10 ng/ml and 24 ng/ml) of blocking antibody treatment also led to an increase in colony sizes [both center (+) and center (–) types] (Fig. 5D), indicating a 'delay' in the timing of the appearance of patterning. Conversely, treatment with an integrin  $\beta$ 1-activating antibody (P4G11; see Materials and Methods) reduced the colony sizes when patterning started to emerge (Fig. 5E). Collectively, these data suggest that integrin-mediated signaling plays a positive role in promoting the pluripotency exit. We next asked how E-cad-mediated cell-cell interaction was involved in this process. hiPSC colonies treated with EGTA (2 mM) for 20 min still retained overall integrity (Fig. 5F, left panels), although cells had rounded-up morphology and longer treatment led to cell detachment. Interestingly, a 20 min EGTA treatment completely abolished patterned expression of pluripotency markers in large colonies, resulting in uniform salt-and-pepper expression of POU5F1 and eliminating the difference between central and pericentral territories (Fig. 5G,H; Fig. 5I, EGTA top). This loss of patterning was not rescued even after 3 h recovery in normal medium (Fig. 5I, EGTA bottom). Because EGTA blocks both E-cad (cell-cell) and integrin (cell-matrix) signaling, we tested the effect of EGTA treatment in the presence of  $Mg^{2+}$  (5 mM) or combined  $Mg^{2+}$  (2.5 mM) and  $Mn^{2+}$  (2.5 mM). Both  $Mg^{2+}$  and  $Mn^{2+}$  are known to specifically promote integrin-mediating signaling (Shimaoka et al., 2002). Addition of  $Mg^{2+}$  did not rescue the effect of 20 min EGTA treatment (Fig. 5G,H; Fig. 5I, top), but did rescue the control pattern after 3 h recovery (Fig. 5I, bottom). Combination of  $Mg^{2+}$  and  $Mn^{2+}$  very robustly inhibited the effect of EGTA (Fig. 5G-I), suggesting that pluripotency exit seen in the center of normal colonies was primarily mediated through integrin signaling. Further supporting our hiPSC-based observations, in early chick embryos, in which pluripotency markers were ubiquitously expressed in the epiblast (Fig. 5K, control; Fig. S3A and Fig. 5L) and pluripotent cells were of partial epithelial morphology (Fig. 1), brief activation of the integrin signaling (EGTA+  $Mg^{2+}$ + $Mn^{2+}$ ) also led to dramatic reduction of NANOG expression (experimental outline in Fig. 5J; NANOG mRNA in Fig. 5K, right; NANOG protein in Fig. 5N).

#### MET-mediated hiPSC pluripotency exit involves canonical EMT/MET-associated transcriptional regulator

The above data suggest that epiblast pluripotency regulation is tightly coordinated with epiblast MET regulation. As in any EMT/MET process, epiblast MET is presumed to be under stereotypical transcriptional regulation. Among the core EMT/MET-associated transcriptional regulators (SNAI1, SNAI2, ZEB1, ZEB2, TWIST1 and TWIST2) (Stemmler et al., 2019), data from geo-profiles suggest that SNAI1, ZEB1 and ZEB2 are highly expressed in hiPSCs (Yagi et al., 2011). We confirmed high expression of SNAI1 in hiPSCs by RNA *in situ* hybridization analysis (Fig. 6A). Interestingly, SNAI1 expression also showed robust patterning in large colonies (Fig. 6A, middle), similar to that of pluripotency markers. SNAI2 expression was very low or negative in hiPSCs (Fig. 6A, right). This colony size-dependent patterning of SNAI1 expression was also seen at the protein level, with pan-colony expression in smaller colonies (Fig. 6B, top) and patterned (center-

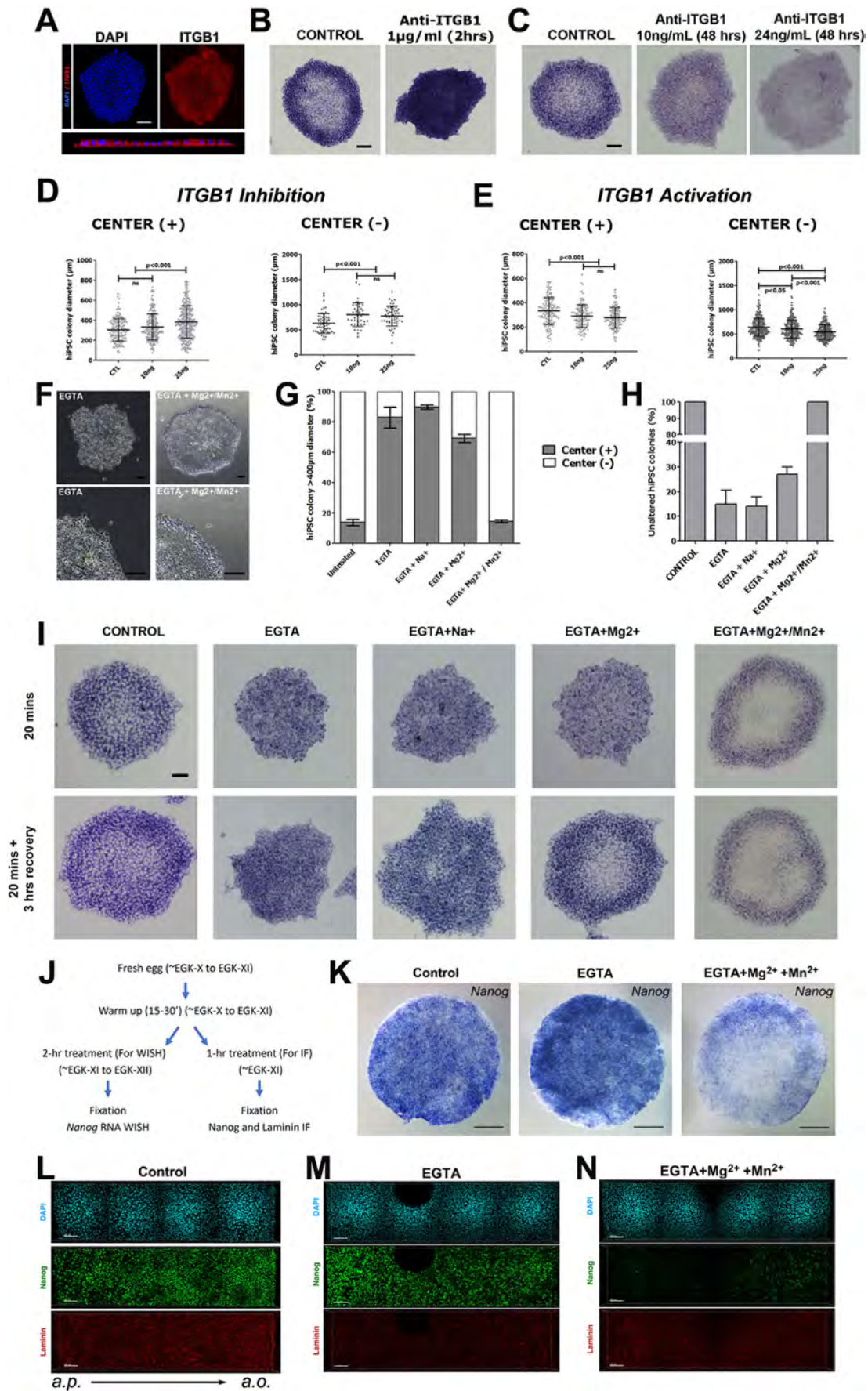


Fig. 5. See next page for legend.

**Fig. 5. Integrin signaling regulates pluripotency exit.** (A) Representative image of integrin- $\beta 1$  (ITGB1) expression in large hiPSC colonies, corresponding to the sum of the images of a confocal acquired stack (step 0.75  $\mu\text{m}$ ), and related reconstructed median optical cross-section of this colony. (B-E) *In situ* hybridization visualization of POU5F1 mRNA expression under control and ITGB1 perturbation conditions. (B) hiPSC colonies treated with ITGB1 blocking antibody for 2 h at 100 ng/ml. POU5F1 RNA *in situ*. (C) hiPSC were cultured in the presence of 10 ng/ml or 25 ng/ml of ITGB1 blocking antibody for 48 h. POU5f1 RNA *in situ*. (D) Analysis of the mean colony diameter of center (-) and center (+) hiPSC colonies. Addition of 10 or 25 ng/ml of ITGB1-blocking antibody significantly increased the mean size of center (-) and center (+) colonies ( $P < 0.001$ ), suggesting that hiPSC epithelialization was initiated in smaller colonies. (E) Analysis of the mean colony diameter of center (-) and center (+) hiPSC colonies after addition of ITGB1-activating antibody (10 or 25 ng/ml for 48 h). Contrary to ITGB1-blocking antibody, ITGB1-activating antibody decreased the mean size of center (-) and center (+) colonies ( $P < 0.001$ ), suggesting that hiPSC epithelialization was initiated in smaller colonies. (F) Bright-field views of hiPSC colonies 20 min after treatment either with EGTA alone or with EGTA and  $\text{Mg}^{2+}/\text{Mn}^{2+}$ . Bottom panels provide magnified views. (G-I) Representative images (I) and quantification (G,H) of POU5F1 mRNA expression in hiPSC colonies after a 20 min treatment with EGTA alone, EGTA and  $\text{Na}^+$  together, EGTA and  $\text{Mg}^{2+}$  together or EGTA and  $\text{Mg}^{2+}/\text{Mn}^{2+}$  together compared with the control (left most panel). Top: 20 min treatment. Bottom: 20 min treatment followed by 3 h recovery in normal culture medium. (J) Schematic diagram of treatment of chicken embryos with EGTA plus  $\text{Mg}^{2+}/\text{Mn}^{2+}$  treatment. Freshly laid eggs were warmed for 15-30 min, followed by New culture incubation for 2 h with albumen replaced by either PBS(+) (control), 2 mM EGTA in PBS(+) or 2 mM EGTA plus  $\text{Mg}^{2+}/\text{Mn}^{2+}$  in PBS(+). Embryos were then fixed for whole-mount *in situ* hybridization or immunofluorescence analysis. Both the start and end stages were categorized as early HH1. (K) EGTA plus  $\text{Mg}^{2+}/\text{Mn}^{2+}$  treatment (right) greatly reduced pluripotency marker NANOG expression in the area pellucida (central epiblast). EGTA-only treatment (center) did not have a prominent effect on NANOG expression. (L-N) Immunofluorescence analysis of an embryo treated with NANOG and laminin antibodies. NANOG protein expression levels were greatly reduced in 2 mM EGTA plus  $\text{Mg}^{2+}/\text{Mn}^{2+}$ -treated embryos (N), whereas EGTA alone had no prominent effect on NANOG protein expression. With either EGTA alone or EGTA plus  $\text{Mg}^{2+}/\text{Mn}^{2+}$  treatment, the basement membrane (laminin) resembled the control case. Scale bars: 100  $\mu\text{m}$  in A-C, I,L-N; 1 mm in K.

low and periphery-high) expression in larger colonies (Fig. 6B, bottom). Aside from the core EMT/MET-associated transcription factors, additional transcriptional regulators are known to play a role in EMT/MET-associated in a process-specific manner and we tested three (GRHL2, YAP and TAZ) among those. GRHL2 was shown to recruit polycomb repressor complex and suppress ZEB1/2 and other EMT-related genes (Chung et al., 2016; Cieply et al., 2012; Mooney et al., 2017), and its downregulation was associated with poor prognosis in individuals with ovarian cancer (Chung et al., 2016; Nieto et al., 2016). Immunofluorescence staining showed that GRHL2 was highly expressed in hiPSCs, but without exhibiting marked regional difference (Fig. 6C). We furthermore tested YAP and TAZ, which are Hippo pathway effectors (Plouffe et al., 2018) and are known to be involved in EMT regulation (Stemmler et al., 2019). Nuclear localization of YAP was shown to positively control epiblast pluripotency in both human and mouse models (Hashimoto and Sasaki, 2018 preprint; Qin et al., 2016). Immunofluorescence staining showed that YAP was expressed and localized to the nucleus in all hiPSCs (Fig. 6D), with a slight decrease in center cells. TAZ was shown to differentially affect the self-renewal and differentiation of primed PSCs via its subcellular localization (Zhou et al., 2017). Consistent with a reported role for nuclear TAZ in promoting EMT, immunofluorescence staining with hiPSCs revealed a prominent difference in TAZ subcellular distribution, with pericenter cells having a nuclear localization and center cells having a cytoplasmic localization (Fig. 6D,E) (Lei et al., 2008).

Both SNAI1 and TAZ were speculated to promote cancer EMT through their regulation of matrix metalloproteinases (MMPs), especially MMP9 (Wu et al., 2017; Xiao et al., 2015). We investigated MMP2 and MMP9 activities (both of which are expressed in hiPSCs based on microarray data) in hiPSC colonies using sequence-specific MMP fluorescent sensors (Lee et al., 2009; Sharma et al., 2013) (see Materials and Methods). MMP9 activity was high throughout the hiPSC colony (Fig. 6G), whereas MMP2 activity was relatively weak but detectable (Fig. 6G). As a negative control, MMP13 activity was not detectable in hiPSCs (Fig. 6G). However, neither MMP9 nor MMP2 exhibited prominent patterning in their activity distribution, suggesting that MMP activity is not the primary target of epiblast MET regulation. This was supported by the observation that treatment with marimastat, a pan-MMP inhibitor, did not lead to significant alteration in POU5F1 patterning in hiPSCs (Fig. 6F). Taken together, these data suggest that several EMT/MET-associated transcriptional regulators are involved in the epiblast MET process. How epiblast MET is transcriptionally regulated remains to be clarified.

#### MET-like colony patterning is also observed in human ESCs, but not in mouse PSCs

We next investigated whether MET-like colony patterning could be observed in other PSCs. Human ESCs (hESCs) were reported to exhibit prepatterning when grown for 24 h in micropatterned culture condition (Warmflash et al., 2014) with colony size-dependent center-low/periphery-high intra-colony variation in pluripotency marker (NANOG, OCT4 and SOX2) expression. This observation was confirmed when hESCs were cultured in pluripotency, maintaining a micropatterned culture condition for either a shorter (11 h; MP-media11 h) or a longer (45 h; MP-media45 h) time period (Fig. 7A, top; Fig. 7B), with more prominent pre-patterning (periphery high, center low) of NANOG, POU5F1 (OCT4) than SOX2 seen after 45 h in culture (Fig. 7B). Such pre-patterning of pluripotency markers (NANOG and POU5F1) was also observed in hESCs cultured under non-micropatterning condition (Dish-media45h; Fig. 7A, bottom; Fig. 7B). These data suggest that intra-colony pre-patterning is a general behavior of human PSCs. Supporting this, hESC colonies also exhibited a prepatterning of EMT/MET marker SNAI1 (Fig. 7A,B), as seen in hiPSC colonies (Fig. 6A,B). This MET-like prepatterning of hESC colonies under maintenance conditions is likely different from EMT-like behavior of hESCs induced under BMP-induced differentiation (Deglincerti et al., 2016b; Warmflash et al., 2014). Under BMP-induced differentiation, SNAI1 was highly expressed in colony periphery, and pluripotency markers NANOG and SOX2 were markedly reduced in this region (MP-BMP45h; Fig. S5). Because SOX2 marks both the pluripotent cell population and the neuroectoderm cell lineage, a differentiating hESC colony would show an upregulation, instead of downregulation, of SOX2 in colony center. Under pluripotency maintenance conditions, reduced NANOG and OCT4 expression in colony center was prominent in both hESCs (Fig. 7A,B) and hiPSCs (Fig. 7C-E) and this was coupled with a mild decrease in SOX2 (Fig. 7) rather than differentiation-associated increase (Fig. S5), suggesting that pluripotency exit is not correlated with spontaneous differentiation.

The hiPSCs have a transcriptome profile similar to post-implantation epiblast and EpiSCs (Nakamura et al., 2016). *In vivo*, epithelialization of the epiblast corresponds to developmental progression from pre-implantation to post-implantation epiblast (Kinoshita and Smith, 2018). We then asked whether similar prepatterning could be observed in mouse EpiSCs (mEpiSCs).

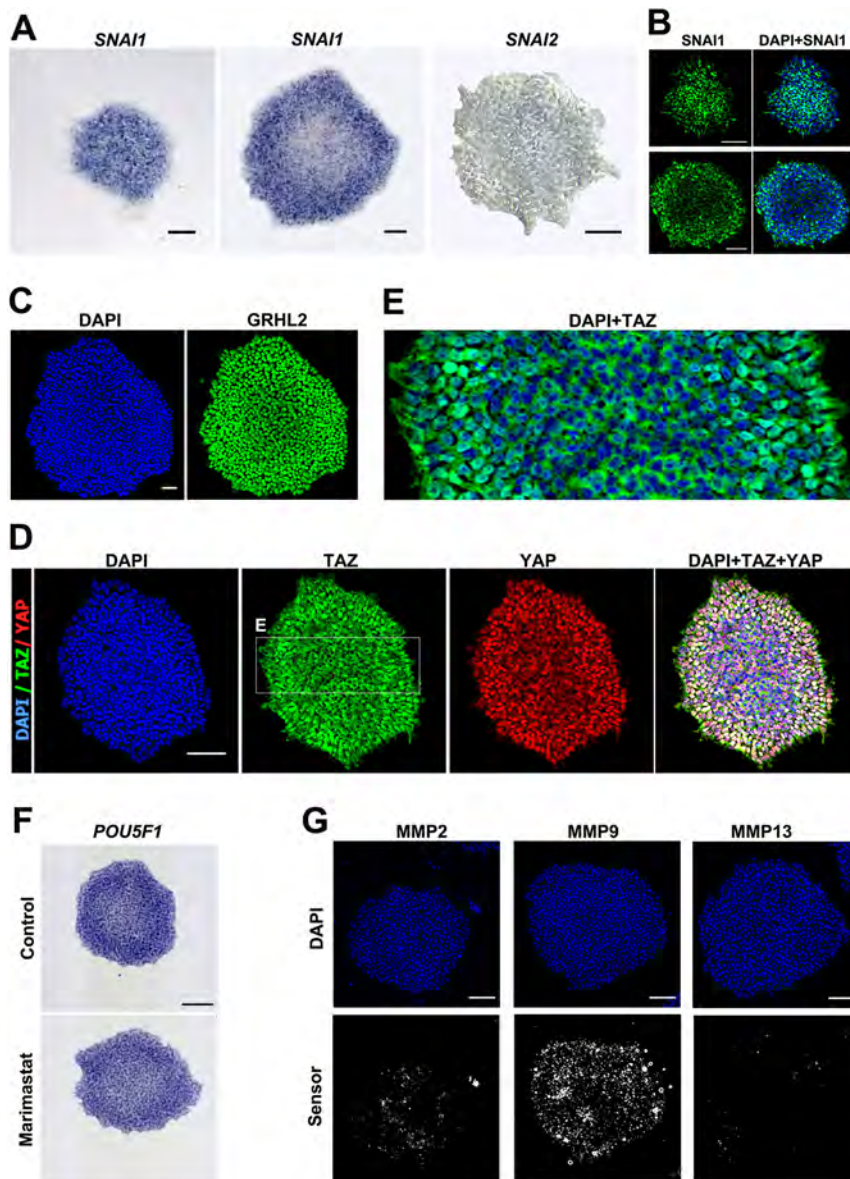


**Fig. 6. Expression of EMT-related regulators and MMPs in hiPSC colonies.** (A) RNA *in situ* hybridization analysis of SNAI1 (Snail) and SNAI2 (Slug). SNAI2 (right) is absent or weakly expressed and SNAI1 (left and middle) is robustly expressed in hiPSC colonies. SNAI1 expression is also patterned (center low and pericenter high) in large colonies (middle). (B) Immunofluorescence staining of SNAI1, showing uniform expression in small hiPSC colonies and patterned expression (center low and pericenter high) in large colonies. (C) Immunofluorescence staining of GRHL2, showing uniform expression. (D) Immunofluorescence staining of YAP and TAZ, showing uniform expression and subcellular localization of YAP, and a clear shift in subcellular localization for TAZ (cytoplasmic in colony center and nuclear in colony pericenter). (E) Magnified view of TAZ (green) and nuclei (cyan), showing the difference in its subcellular localization between colony center and pericenter regions. (F) POU5F1 RNA expression is not affected by the pan-MMP inhibitor marimastat. (G) Activities of MMPs detected in hiPSCs using specific MMP sensors for MMP2, MMP9 and MMP13 (see also Materials and Methods). MMP9 is highly active, MMP2 is weakly active and MMP13 is not active. However, intra-colony epithelialization pattern is not reflected in the MMP2 activity distribution pattern. Scale bars: 100  $\mu$ m in A-D,F,G.

We first checked epithelial status of mEpiSC and mESC colonies (Fig. 8A,B). The mEpiSC colony (Fig. 8B) had a single cell-layered structure with well-localized ZO-1 (tight junction) and E-cad (adherens junction), with no obvious regional variation, indicating its full epithelial organization. In contrast, mESC colony had a multilayered structure with irregular E-cad and ZO-1 signals (Fig. 8A). mESCs had higher levels of expression of pluripotency markers NANOG and POU5F1 at both the protein (Fig. 8C) and RNA (Fig. 8D) levels. But no intra-colony pre-patterning could be observed in either mEpiSC or mESC colonies. Our mEpiSCs were cultured in the presence of a Wnt inhibitor that was known to reduce heterogeneity in NANOG expression levels. However, even when cultured in the absence of Wnt inhibitor, mEpiSCs did not exhibit pre-patterning in NANOG or POU5F1 levels (Fig. 8G), or show marked difference in their epithelial marker (ZO-1 and E-cad) localization (Fig. 8H). Similar to hiPSCs, GRHL2 was expressed in all cells in both mEpiSC and mESC colonies, but without any overt patterning (Fig. 8E). Interestingly, we did observe a prominent difference in SNAI1 subcellular localization, with predominantly cytoplasmic localization in mESCs and predominantly nuclear

localization in mEpiSCs. Taken together, these data suggest that, in mouse PSCs under the current culture conditions, differential epithelialization status and pluripotency level are not reflected as intra-colony pre-patterning, but rather as differences in colony morphology and pluripotency regulation between mESCs and mEpiSCs.

## DISCUSSION

The avian embryo before gastrulation contains three lineages: the epiblast, hypoblast and area opaca (Fig. 9A, left). The first two are equivalent to their mammalian counterparts (Fig. 9A, right). The third anchors the developing embryo to the yolk and stretches the epiblast as it expands over the yolk surface. The area opaca cells are also the evolutionary origin of mammalian trophoblasts. The monotremes, the earliest branched-out extant mammals, for example, still retain an avian-like pre-gastrula organization (Sheng, 2015). Despite the superficial difference in epiblast topography between chick (exposed to the embryo exterior) and human (covered by polar trophectoderm), epiblast cells in both species undergo a very similar sequence of molecular and morphogenetic

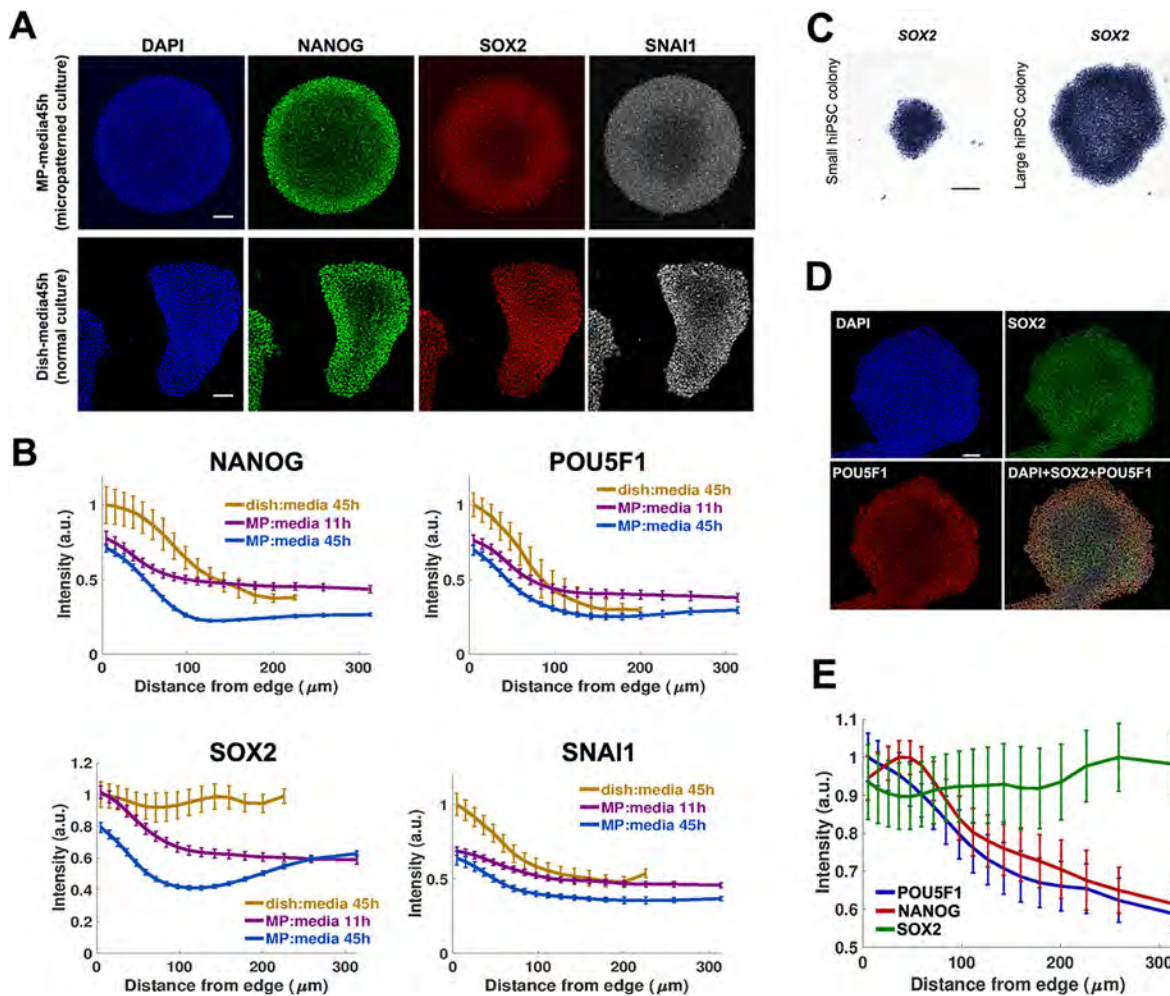


**Fig. 7. hESCs exhibit similar intra-colony patterning of pluripotency and EMT markers.** (A) hESCs were seeded and cultured for 45 h in either micropatterning (MP-media45 h) or normal (Dish-media45 h) conditions (see Materials and Methods for details). Colonies were stained for NANOG, SOX2 and SNAI1. Similar to hiPSCs, a pattern of center-low and periphery-high expression could be observed for all three markers. (B) Statistical analysis of data shown in A. An additional marker (POU5F1) and culture condition (11 h in micro-patterning conditions) [MP-media11 h] are also included in the analysis. Under non-differentiation culture conditions (Dish-media45 h and MP-media45 h and MP-media11 h), a center-low/periphery-high pattern of expression could be seen for NANOG, POU5F1, SOX2 and SNAI1. (C) SOX2 mRNA expression in small (left) and large (right) colonies. (D) SOX2 protein expression in large colonies (green) co-stained for POU5F1 (red). (E) Statistical analysis of data shown in D. The additional marker NANOG is also included in the graph. Both NANOG and POU5F1 have prominent pericenter-high and center-low pattern. In either hiPSCs or hESCs, SOX2 does not show upregulation in the colony center, suggesting that these cells are not differentiating into neuroectoderm lineage (as seen with center cells under induced differentiation; see Fig. S5). Scale bars: 100  $\mu\text{m}$  in A,C,D.

events (Fig. 9A). These events include: (1) molecular specification of epiblast precursors; (2) morphological sorting of epiblast-fated cells; (3) full epithelialization of the epiblast (subject of this study); (4) morphogenesis of epithelialized epiblast; and (5) dissolution of epithelial structure during gastrulation EMT. It is generally considered that pluripotency loss coincides with the last step in this sequence, when mesendoderm cells switch off pluripotency markers after gastrulation EMT and the remaining epiblast cells differentiate into ectoderm derivatives and, likewise, lose pluripotency. In this work, we demonstrate that there is an additional component of pluripotency regulation that is distinct from gastrulation EMT-related pluripotency loss. We termed this process ‘pluripotency exit’ and its earliest step ‘initiation of pluripotency exit’. We provide evidence that this ‘initiation of pluripotency exit’ is correlated with and regulated by epiblast partial MET (Fig. 9A). This partial MET refers to the transition from an immature epithelioid organization to a fully epithelial organization. Using a combination of avian epiblast and mammalian PSC models, our data suggest that partial MET-mediated pluripotency

exit is reversible and is evolutionarily conserved. It is primarily regulated through the specification of the basal membrane domain of the epiblast and by integrin-mediated epiblast-extracellular matrix signaling.

The process of epiblast pluripotency exit described in this work is likely different from the ‘naïve-to-primed’ transition that has been reported in the mouse (Shahbazi et al., 2017) (Fig. 9B). The basic distinctions between these two *in vitro* (naïve and primed) states of pluripotency are their *in vitro* culture conditions and *in vivo* reconstitution potentials. The naïve state has been hypothesized to represent the pre-implantation epiblast, whereas the primed state represents the post-implantation state (Nichols and Smith, 2009). Cell biological studies suggest that this transition is associated with polarization of the mouse and human epiblast (Shahbazi et al., 2017). However, our study showed that in both chicken epiblast at EGK-X (oviposition stage) and young hiPSC colonies, the pluripotent stem cells are already polarized in their apical-basolateral axis, suggesting that the starting point of our analysis

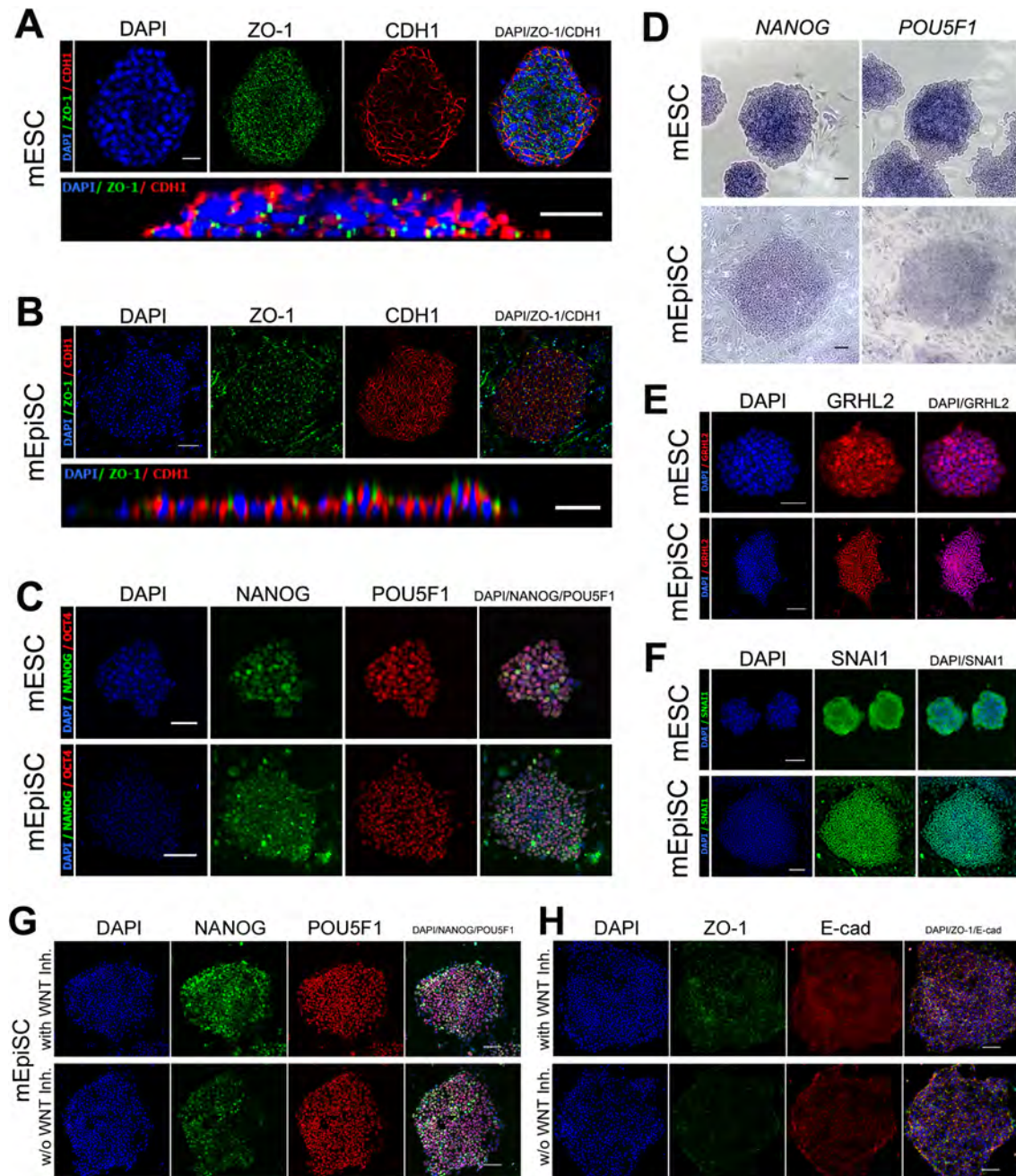


**Fig. 8. Mouse ESCs and mouse EpiSCs represent two extremes of morphological diversity in PSCs.** Mouse EpiSCs (mEpiSCs) were organized as an epithelial structure and expressed lower levels of pluripotency markers. Mouse ESCs (mESCs) were organized as a multilayer non-epithelial structure and expressed higher levels of pluripotency markers. (A) mESC colonies were immunostained for ZO-1 and CDH1 (E-cad). mESC colonies expressed both ZO-1 and CDH1, and exhibited multilayered organization. Both ZO-1 and CDH1 were poorly localized and mESCs were not organized as an epithelial structure. (B) mEpiSC colonies were immunostained for ZO-1 and CDH1 (E-cad). mEpiSC colonies exhibited single-cell layered epithelial organization, with proper junctional localization of ZO-1 and CDH1. (C) Pluripotency markers (NANOG and POU5F1) did not exhibit intra-colony patterning in mPSCs. However, protein expression levels of NANOG and POU5F1 were higher in mESCs than in mEpiSCs. (D) RNA *in situ* hybridization analysis of NANOG and POU5F1 in mESCs and mEpiSCs. RNA expression levels were higher in mESCs than in mEpiSCs. (E, F) Immunofluorescence staining of mESCs and mEpiSCs using GRHL2 and SNAI1 antibodies. Neither GRHL2 (E) nor SNAI1 (F) showed prominent intra-colony patterning. However, SNAI1 was seen to be localized in the cytoplasm in mESCs and in the nucleus in mEpiSCs. (G, H) mEpiSCs cultured in the presence (top) or absence (bottom) of the Wnt inhibitor (XAV939; 10 μM), and stained for NANOG and POU5F1 (G) or for ZO-1 and E-cad (H). No pre patterning for NANOG or POU5F1 is observed under either condition. Scale bars: 50 μm in A-H; A, C, E, F (top) and B (bottom); 25 μm in A (bottom); 100 μm in B (top), C, E, F (bottom) and D, G, H.

is a primed-like state of pluripotency. This hypothesis is supported by molecular data from hiPSCs (showing a primed pluripotency signature) and from our comparative analysis of pluripotency markers in two avian species: the zebra finch (oviposition at EGK-VI; with a prominent naïve pluripotency signature) and chick

(oviposition at EGK-X; with a primed pluripotency signature) (Mak et al., 2015). Despite such distinctions, the ‘naïve-to-primed’ transition and the ‘pluripotency exit’ reported here likely represent the same sequence of events in epiblast MET (Fig. 9A,B), with the former corresponding to the first half of MET (from non-polarized



are the major  $\alpha$  subunits. Interestingly, integrin profiling of the 201B7 line (Table S3) suggests that such heterogeneity is conserved in hiPSCs, which express ITGB1, ITGB5, ITGAV, ITGA6 and ITGAE as their major  $\alpha$  and  $\beta$  subunits. Involvement of integrin signaling in pluripotency cell maintenance has been reported. For example, integrin-mediated focal adhesion kinase activity has been shown to protect hESCs from apoptosis and differentiation (Vitillo et al., 2016), and  $\alpha v \beta 5$  integrin supports self-renewal of hESCs (Braam et al., 2008). Furthermore,  $\alpha 6 \beta 1$  has been shown to mediate laminin 511-supported renewal of hESCs and hiPSCs (Rodin et al., 2010), but likely through  $\alpha 6$ -mediated suppression of  $\beta 1$ -integrin activity, as activation of  $\beta 1$ -integrin or knockdown of  $\alpha 6$ -integrin led to a reduction of pluripotency marker expression (Villa-Diaz et al., 2016). Supporting this, inhibition of integrin signaling by disintegrin could promote pluripotency maintenance of mouse iPSCs (Higuchi et al., 2016). In our work, brief suppression of integrin signaling using high concentrations of  $\beta 1$ -integrin blocking antibody resulted in a dramatic increase in pluripotency level and in the blockage of pluripotency exit (Fig. 5B), and brief activation of integrin signaling using  $Mg^{2+}$  and  $Mn^{2+}$  led to pluripotency exit in both hiPSCs (Fig. 5F) and chicken embryos (Fig. 5K,N), strongly suggesting that the MET-associated pluripotency exit observed in our model systems is positively regulated by integrin signaling. However, our results also point to a putatively positive role of integrin signaling in pluripotency maintenance, because long-term treatment of low concentrations of  $\beta 1$ -integrin blocking antibody resulted in a reduction of pluripotency marker expression (Fig. 5C). Future experiments on how integrin signaling is transmitted intracellularly to regulate the pluripotency network will be needed to clarify such discrepancy.

Our work is the first to associate epiblast cell morphology with epiblast pluripotency exit in embryonic epiblast and cultured PSCs. It is unclear whether this phenomenon can be generalized to all cultured pluripotent cells that adopt an epithelial-like colony structure during their maintenance phase or whether it reflects intrinsic morphogenetic behavior of their developmental origin: the epiblast. We did not observe intra-colony MET in mEpiSCs, although these cells adopt a perfect epithelial morphology throughout the colony. Such species-specific differences may be due to differences in culture conditions, but it also suggests that morphological features are not the sole indicator of variability in the pluripotency spectrum. Patterned heterogeneity in pluripotency marker expression was proposed to facilitate higher-order patterning under differentiation conditions in human ESCs and mouse epiblast-like cells (Deglincerti et al., 2016b; Morgani et al., 2018; Warmflash et al., 2014), possibly by facilitating lineage-specific gene expression through GRHL2-mediated enhancer switching in the regulation of pluripotency genes (Chen et al., 2018). As MET-like pre-patterning was also observed in hESC colonies, it would be interesting to test in the future whether differences in differentiation potentials can also be associated with cells isolated from sub-regions of the hESC colony with different epithelialization status and EMT/MET marker expression levels. Such a hypothesis is supported by a recent paper showing that intra-colony difference in cellular adhesive properties defines a potential N-cad<sup>+</sup> founder cell population within primate PSC colonies (Nakanishi et al., 2019).

More importantly, as we have demonstrated, pluripotency exit is reversible and is different from pluripotency loss seen during gastrulation *in vivo* or under differentiation conditions *in vitro*. For ectoderm-fated epiblast cells, the MET is clearly necessary because both neural ectoderm and non-neural ectoderm cells adopt a fully epithelial morphology after gastrulation. For those epiblast cells that

will eventually give rise to the mesoderm and endoderm germ layers during gastrulation, they will have to undergo a MET to achieve full epithelial status only to be followed by a full EMT and loss of their pluripotency. The biological significance of such morphogenetic behavior is unclear because, *in vitro*, lineage differentiation into the three germ layers can be achieved from pluripotent cells regardless of their epithelialization status (Fig. 9B). Although the term epiblast generally refers to pluripotent cells in amniotic vertebrates (birds, reptiles and mammals), the pluripotency regulatory network has deep evolutionary root (Niwa et al., 2016) and similar pluripotent cells also exist in the anamniotic vertebrates [e.g. in zebrafish (Robles et al., 2011; Rosselló et al., 2013)]. It is therefore interesting to note that full epithelialization of pre-gastrulation pluripotent cells only occurs within the amniote clade (Nakaya and Sheng, 2008; Sheng, 2015). This suggests that epiblast MET is associated with certain amniote-specific developmental features that require epithelial structure-based intercellular signaling or force transmission [e.g. epiblast cell intercalation and polonaise movement reported in the pre-gastrulation chick embryo (Chuai et al., 2006; Hamidi et al., 2019; Voiculescu et al., 2007)]. These epithelial structure-based cellular events are known to be directly involved in the formation of the primitive streak (an amniote-specific feature) or, more generally, of a posterior epiblast-restricted center of mesendoderm internalization (i.e. of later-on gastrulation EMT). Therefore, epiblast MET is not only important for epiblast pluripotency regulation, as described in this work, but likely also for epiblast planar symmetry breaking. How these two phenomena are linked developmentally remains to be clarified.

## MATERIALS AND METHODS

### Array analysis of chicken area pellucida samples

Fertilized chicken eggs purchased from a local farm (Shiroyama farm, Kanagawa, Japan) were incubated without storage at 38.5°C for 0.5, 5.5, 9 and 14 h. The area pellucida (AP) region of the embryos, containing both the epiblast and hypoblast, but excluding the primitive streak region for 9 h and 14 h sample sets, was cut out in Pannett-Compton solution. Dissected AP samples of specific time points were pooled and used for RNA isolation. Two independent sets of total RNA from pooled AP samples were isolated using QIAGEN RNeasy Micro Kit. Quality checked total RNAs (100 ng) were used for array analysis, with the cDNA synthesis and cRNA labeling reactions performed according to the two-cycle protocol provided by Affymetrix. Affymetrix high-density oligonucleotide arrays for *Gallus gallus* (GeneChip Chicken Genome) were hybridized, stained and washed according to the Expression Analysis Technical Manual (Affymetrix), and analysis of resulting expression values was performed as described previously (Alev et al., 2010). Raw array data have been deposited in GEO under accession number GSE114476.

### hiPSC culture and reagents

The hiPSC line 201B7 (purchased from RIKEN BRC Cell Bank) was used for all experiments. Cells were maintained in an undifferentiated state on iMatrix-511 (0.5  $\mu\text{g}/\text{cm}^2$ ; Nippi; 892018)-coated dishes using the StemFit AK02N (Ajinomoto) medium and cultured at 37°C with 5% CO<sub>2</sub>. At day 7 of culture, hiPSC colonies were dissociated using accutase (Nacalai tesque, 12679-54) and unicellular hiPSCs were then seeded on new culture dishes freshly coated with iMatrix-511, in a medium containing 10  $\mu\text{M}$  Y-27632 (Wako Pure Chemicals Industries, 253-00513). All experiments in this study were performed at day 6 of culture, 1 day before normal passaging. For pattern alteration experiments, Y-27632 was used at a concentration of 20  $\mu\text{M}$ , MMP broad spectrum inhibitor Marimastat (a gift from Prof. Hiroshi Sato, Kanazawa University, Japan) at 150 nM, nocodazole (Wako, 140-08531) at 10  $\mu\text{g}/\text{ml}$ , EGTA (Sigma, E3889) at 2 mM, MgCl<sub>2</sub> (Sigma, 1901905) at 5 mM when alone or at 2.5 mM when associated with MnCl<sub>2</sub> (2.5 mM; Wako, 139-00722) and NaCl at 5 mM (Wako, 195-01663). Monoclonal antibody against  $\beta 1$ -integrin (inhibiting antibody clone P5D2

or activating antibody clone P4G11; Developmental Studies Hybridoma Bank AB528308 or AB528307) was added to the culture media either at day 4 of culture at concentrations of 10 ng/ml and 25 ng/ml or for only 2 h prior to fixation at 1 µg/ml.

#### hESC culture

ES017 hESCs were grown in mTeSR1 (STEMCELL Technologies) in tissue culture dishes coated with Matrigel (Corning; 1:200 in DMEMF12) overnight at 4°C. Cells were passaged using dispase (STEMCELL Technologies) every 3 days. Cells were routinely tested for mycoplasma contamination and found negative. Micropatterning experiments were also performed with mTeSR1 following the protocol previously described (Deglincerti et al., 2016a). Where indicated, cells were treated with 50 ng/ml BMP4 to induce differentiation.

#### mPSC culture

The mESC line EB5 was grown on 0.1% gelatin-coated dishes in a medium consisting of GMEM 10% knockout serum replacement, 1% FBS, 1 mM sodium pyruvate (Wako, 190-14881), 1× non-essential amino acids (Sigma M7145) and LIF 1000 U/ml. Cells were passaged every 3 days using accutase. The mEpiSC line (Tesar et al., 2007) was grown on 0.5 µg/cm<sup>2</sup> iMatrix-511 (Nippi)-coated dishes in a medium consisting of DMEM-F12, 20% knockout serum replacement, 1 mM sodium pyruvate, 1× non-essential amino acids, 10<sup>-4</sup> M 2-ME, 10 ng/ml activin A (R&D Systems, 338-AC), 5 ng/ml human recombinant FGF2 (R&D Systems, 3139-FB) and 10 µM of XAV939 (Abcam, ab120897). Cells were passaged every 4-5 days using accutase for single cell dissociation.

#### Laser microdissection

hiPSC colonies were grown on plasma-treated glass-bottomed dish coated with iMatrix-511. At day 6, the periphery and center of patterned colonies were separated using the laser beam of a Zeiss PALM microbeam. Following laser microdissection, both regions were isolated manually under a microscope. Selected cells were treated with Y-27632 for 2 h prior to dissociation and re-plated either at a density of 200 cells/cm<sup>2</sup> for pluripotency assessment experiments or at 400 cells/well (Prime Surface 96V Sumilon Sumitomo Bakelite, Wako, MS-9096V) for differentiation experiments.

#### hiPSC differentiation and PCR analysis

After 5 days of culture, newly formed embryoid body differentiation was induced by replacing maintenance media with DMEM 10% FBS. After 3 days, samples were collected for RNA extraction (RNeasy micro Kit, QIAGEN) along with MCF-7, HepG2, HUVEC and undifferentiated hiPSC that were used as positive and negative controls. PCR was performed by using the following primers: human GAPDH, 5'-TCATCCCTGAGCTG-AACGGG-3' (forward) and 5'-TCCCCTCTTCAAGGGGTCTACA-3' (reverse); human NESTIN, 5'-CAGGGTTGGAACAGAGGTTGG-3' (forward) and 5'-GCATCTACAGCAGGAGAGGGTG-3' (reverse); human SOX1, 5'-CGGAGCTCGTCGATTTGTT-3' (forward) and 5'-TCC-CGGGGTTCCTTACTT-3' (reverse); human PAX6, 5'-CACCCG-CCCTGGTTGGTATC-3' (forward) and 5'-TGAGGGCTGTCTCTGTT-CGG-3' (reverse); human FOXA2, 5'-AGCGGTGAAGATGGAAGGG-3' (forward) and 5'-ATGGCCATGGTATGAGCGA-3' (reverse); human T, 5'-CCGAGAGCGGGAAAGAG-3' (forward) and 5'-TCACTATGTG-GATTCGAGGCTCAT-3' (reverse); human HAND1, 5'-TTAACAGCGC-ATTCGCGGAG-3' (forward) and 5'-CGTGCATCAAGT-GTGTGG-3' (reverse); human EOMES, 5'-ACACTTTACCTCAAGCCCGC-3' (forward) and 5'-AGTTGCTAGGAGACAGCCGC-3' (reverse); human GATA4, 5'-GTCCCAGTGCAGACCTGCTG-3' (forward) and 5'-CCCTGAGGC-TGTAGGTTGTG-3' (reverse); human CDX2, 5'-CTTCTGCGCTT-CTGGGCT-3' (forward) and 5'-CCAGGCACTGAGGCTTGC-3' (reverse).

#### In situ hybridization

Probes used for *in situ* hybridization were as follows: human NANOG, 5'-GTGTGGATCCAGCTGTCC-3' (forward) and 5'-GTACACCATGCTATTCTTC-3' (reverse) 493 bp; human POU5F1, 5'-CAAGAACATGT-

GTAAGCTGCGG-3' (forward) and 5'-AGGAGTACAGTGCAGTG-AAG-TG-3' (reverse) 425 bp; human LEF1, 5'-CCAGACAAGCACAAACCTCT-C-3' (forward) and 5'-AGCCAAGAGGTGGGGTGATC-3' (reverse) 420 bp; human OTX2, 5'-GAGAGGACGACGTTCACTC-3' (forward) and 5'-TC-TGACAGTGGGGAGATGG-3' (reverse) 365 bp; human SNAIL, 5'-TGCC-TCGACCACTATGCCG-3' (forward) and 5'-AGGCTCGAAAGGCCTTC-AACT-3' (reverse) 479 bp; human SNAIL2, 5'-TTCGTAAAGGAGCCGG-GTGAC-3' (forward) and 5'-ATCTTTGGGGCGAGTGAGTCC-3' (reverse) 425 bp; human CLDN6, 5'-ACTCGGCCTAGGAATTCCTT-3' (forward) and 5'-TAATCCCCGTGTGCTGG-ACG-3' (reverse) 473 bp; human MMP2, 5'-TCTTTGGACTGCCCCAGACA-3' (forward) and 5'-AGTACTCCCCA-TCGGCGTTC-3' (reverse) 447 bp; human MMP9, 5'-AAGGCCAATCCT-ACTCCGCC-3' (forward) and 5'-AGGGCGAGGACCATAGAGGT-3' (reverse) 445 bp; mouse POU5F1, 5'-CAGGACATGAAAGCCCTGCAG-AA-3' (forward) and 5'-GCCCAAGCTGATGGCGAT-3' (reverse) 397 bp; and mouse NANOG, 5'-CTGGGAACGCCTCATCAATGC-3' (forward) and 5'-TACTCCACTGGTGTGAGCC-3' (reverse) 469 bp. *In situ* hybridization was performed as described previously for chick embryos (Nakazawa et al., 2006) with a slight adaptation in incubation time or concentration of reagents. More specifically, cultured cells were fixed in 4% paraformaldehyde overnight at 4°C. A permeabilization step was performed using 1 µg/ml proteinase K incubation for 20 min at room temperature, followed by post-fixation for 15 min, prehybridization at 68°C for 3 h and hybridization with gene-specific antisense DIG-labeled probes at 68°C overnight. After hybridization, samples were washed in prehybridization solution at 68°C and then in TBST at room temperature. This was followed by 1 h blocking at room temperature and overnight incubation in anti-DIG antibody solution (1/2000; Roche, 11093274910) at 4°C. Finally, after several washing steps in NTMT solution, hiPSC colonies were processed for color development in NBT and BCIP at room temperature shielded from light. Whole-mount *in situ* hybridization with chicken embryos for NANOG mRNA detection was carried out as previously described (Nakazawa et al., 2006) and probe information for chicken NANOG has been reported previously (Shin et al., 2011).

#### Imaging and immunofluorescence staining for PSCs

All immunofluorescence experiments were performed using cells grown on plasma-treated glass-bottomed dish. The following primary antibodies were used for NANOG (1:500, ReproCELL, RCAB004P for hiPSCs; 1:200, R&D Systems, AF1997 for hESCs or RCAB001P for mouse PSCs), OCT3/4 (also known as POU5F1; 1:500; BD Transduction Laboratories, 611202), SOX2 (1:200; Cell Signaling, 3579 for hESCs and 1:1000 with rabbit antisera against mouse Sox2), Omni-probe D8 (1:200; Santa Cruz Biotechnology, sc-7270), E-cad (1:500; BD Transduction Laboratories, 610181), ZO-1 (1:100; Invitrogen, 40-2200), β-dystroglycan (1:100; Leica, NCL-b-DG), aPKCζ clone C-20 (1:400; Santa Cruz Biotechnology, sc-216), β1-integrin clone P5D2 (1:100; Developmental Studies Hybridoma Bank, AB528308), LAMA1 (1:200, Sigma, L9393), HSPG2 (1:200, Millipore, MABT12), GRHL2 (1:500, Sigma, HPA004820), SNAIL (1:200, R&D Systems, AF3639), YAP (1:100, Santa Cruz Biotechnology, sc-101199) and TAZ (1:100, Atlas Antibodies, HPA007415) (both YAP and TAZ antibodies were kindly provided by Dr K. Nishiyama of Kumamoto University, Japan). The following secondary antibodies were used for multicolor detection: Alexa Fluor 488 and 568 (1:850; Invitrogen), except for hESCs, where secondary antibodies were used at a concentration of 1:500 (Alexa Fluor 488, 555 and 647). Images were acquired using an Olympus FV1200-IX-KU laser scanning confocal microscope for all samples except for 3D reconstruction, where a Leica TCS SP8 confocal microscope was used. Single cell 3D reconstruction experiments were generated using the Imaris software v8.0 (Bitplane), and all other image analyses were performed using Fiji software.

#### Imaging and immunofluorescence staining for chicken embryos

Chicken embryos were fixed in 4% PFA. For whole-mount staining of NANOG, embryos were processed for immunofluorescence staining, then cleared with SeeDB 2G tissue-clearing solution (Ke et al., 2016) before being processed for imaging. The following primary antibodies were used: E-cad (1:100; BD Transduction Laboratories, 610181), ZO-1 (1:100; Thermo Fisher, 40-2200), aPKC clone C-20 (1:100; Santa Cruz Biotechnology,

sc-216), GM130 clone 35 (1:100; BD Bioscience, 610822), AcTub clone 6-11B-1 (1:1000; Sigma, T6793),  $\beta$ 1-integrin (1:300; Chemicon, MAB13443), dystroglycan clone H242 (1:100; Santa Cruz Biotechnology, sc-28535), pan-laminin 1 clone 3H11 (1:100; DSHB, AB528342), laminin A1 (1:100; Sigma, L9393), agrin clone 6D2 (1:100; from DSHB) and NANOG (1:500; kindly provided by Dr Agata from Gakushuin University, Japan) (Nakanoh et al., 2015). The following secondary antibodies were used for multicolor detection: Alexa Fluor 488, 568 or 594 (1:300 for whole-mount embryo staining, 1:500 for frozen section staining; Invitrogen). Images were acquired using Olympus FV1000 with BX61WI upright or FV3000RS with IX83 invert laser scanning confocal microscope with UPlan-SApochromat 60 $\times$ /1.2 NA, UPLSAPO 60 $\times$ /1.3 NA or UPLSAPO 30XS/1.05 NA objective lenses.

### hiPSC sample processing and histology

hiPSC line 201B7 was cultured in the same condition as described above but on polycarbonate membrane inserts (Nunc, 140660). At day 6, membranes were washed with PBS and fixed in 4% paraformaldehyde for 15 min, followed by a second washing step using PBS membrane and coating with 1% bovine gelatin (Sigma, G9391) for 1 h at 37°C. Membranes were then washed and fixed again overnight in 4% paraformaldehyde. Counterstaining of hiPSC colonies was carried out using H&E staining reagents. Briefly, membranes were incubated with Meyer-Hematoxylin (Sakura Finetek, 8650) for 5 min and Eosin (Sakura Finetek, 8659) for 2 min. Membranes were then dehydrated using methanol and isopropanol serial baths before paraffin wax permeabilization (3 $\times$ 40 min each). Membranes were then cut away from the inserts using a scalpel and placed in a mold for final paraffin wax-embedded sectioning (10  $\mu$ m). Sections were collected on bovine gelatin-coated slides, dewaxed and mounted. Analysis was performed using an Olympus BX51 microscope equipped with a DP70 digital camera.

### Expression constructs and transfection

The pEF-His-A-derived mammalian expression vector, T7/His epitope-tagged human wild-type PAR1b/MARK2, 'kinase deficient' PAR1b-KM (K49M) and non-phosphorylatable PAR1b-TA (T595A) constructs were kindly provided by Dr Shigeo Ohno (Yokohama City University, Japan) (Masuda-Hirata et al., 2009). All transfections have been performed using the Gene Juice reagent (EMD Millipore, 70967) following the manufacturer's instructions at day 4 of hiPSC culture.

### Synthesis and characterization of MMP2, MMP9 and MMP13 peptide sensors

The MMP sensors consist of MMPs peptide substrate, fluorescence dye (Cyanine 5.5, Ex/Em 675/690 nm) and dark quencher (BHQ-3, abs 650 nm). The MMP2, MMP9 or MMP13 sensor was prepared as previously described (Lee et al., 2009; Sharma et al., 2013). Briefly, Cy5.5 succinimide ester and BHQ-3 succinimide ester were conjugated to the MMP2 (Gly-Pro-Leu-Gly-Val-Arg-Gly-Lys-Gly-Gly), MMP9 (Gly-Lys-Gly-Pro-Arg-Ser-Leu-Ser-Gly-Lys-Gly-Gly) and MMP13 (Gly-Val-Pro-Leu-Ser-Leu-Thr-Met-Gly-Lys-Gly-Gly) substrates, respectively, and purified by reverse-phase high performance liquid chromatography (RP-HPLC). The sensor specificity was confirmed by activated recombinant enzymes (MMP1, MMP2, MMP3, MMP7, MMP9, MMP10 and MMP13) and fluorescence signal was detected using a fluorometer.

### Statistical analysis

Results were expressed as mean $\pm$ s.e.m. Statistical significance was determined using Student's *t*-test, ANOVA with Bonferroni's post-hoc test or Pearson correlation wherever appropriate. Results were considered significant when  $P < 0.05$ .

### Acknowledgements

We thank Ms Eriko Sukowati, Dr Yuping Wu and Ms Ayako Isomura for help with chicken embryology; Dr Hiroki R. Ueda, Ms Junko Nishio and Mr Kenichiro Uno for help with genechip data production; Dr Shigeo Ohno, Dr Tomonori Hirose and Dr Shoukichi Takahama for sharing PAR1b expression constructs; Dr Ruby Huang for sharing GRHL2 antibody; Dr Kiyokazu Agata for sharing chicken NANOG antibody; Dr Koichi Nishiyama for sharing the YAP and TAZ antibodies; Dr Hiroshi

Sato for sharing the MMP inhibitor Marimastat; Ms Yangye Zhang and Mr Galym Ismagulov for help with integrin and EMT marker analysis; and Ms Marina Lizio for help with CAGE data analysis. We also thank the core imaging facility at International Research Center for Medical Sciences, Kumamoto University for help with image acquisition.

### Competing interests

The authors declare no competing or financial interests.

### Author contributions

Conceptualization: S.H., G.S.; Methodology: S.H., Y.N., H. Nagai, C.A., T.K., S.C., R.L., H. Niwa, A.W., T.S., G.S.; Formal analysis: S.H., Y.N., H. Nagai, S.C., H. Niwa, A.W., G.S.; Investigation: S.H., Y.N., H. Nagai, C.A., T.K., S.C.; Resources: C.A., T.K., R.L., H. Niwa, A.W., T.S., G.S.; Writing - original draft: G.S.; Writing - review & editing: S.H., G.S.; Supervision: G.S.; Funding acquisition: G.S.

### Funding

This work was partially supported by the core research grants to G.S. from the RIKEN Center for Developmental Biology and from the International Research Center for Medical Sciences at Kumamoto University; by a post-doctoral fellowship to S.H. from the International Research Center for Medical Sciences, Kumamoto University; and by a Takeda Medical Research Foundation grant and a Japan Society for the Promotion of Science Kakenhi grant to G.S. This work was also supported by a National Science Foundation grant (NSF-MCB1553228) to A.W. and by a Simons Foundation grant (511079) to A.W.

### Data availability

Raw array data have been deposited in GEO under accession number GSE114476.

### Supplementary information

Supplementary information available online at <http://dev.biologists.org/lookup/doi/10.1242/dev.184960.supplemental>

### References

- Alev, C., Wu, Y., Kasukawa, T., Jakt, L. M., Ueda, H. R. and Sheng, G. (2010). Transcriptomic landscape of the primitive streak. *Development* **137**, 2863-2874. doi:10.1242/dev.053462
- Arner, E., Daub, C. O., Vitting-Seerup, K., Andersson, R., Lilje, B., Drablos, F., Lennartsson, A., Rönnerblad, M., Hrydziusko, O., Vitezic, M. et al. (2015). Transcribed enhancers lead waves of coordinated transcription in transitioning mammalian cells. *Science* **347**, 1010-1014. doi:10.1126/science.1259418
- Basilicata, M. F., Frank, M., Solter, D., Brabletz, T. and Stemmler, M. P. (2016). Inappropriate cadherin switching in the mouse epiblast compromises proper signaling between the epiblast and the extraembryonic ectoderm during gastrulation. *Sci. Rep.* **6**, 26562. doi:10.1038/srep26562
- Bedzhov, I. and Zernicka-Goetz, M. (2014). Self-organizing properties of mouse pluripotent cells initiate morphogenesis upon implantation. *Cell* **156**, 1032-1044. doi:10.1016/j.cell.2014.01.023
- Bellairs, R. (1986). The primitive streak. *Anat. Embryol. (Berl)* **174**, 1-14. doi:10.1007/BF00318331
- Blakeley, P., Fogarty, N. M. E., del Valle, I., Wamaitha, S. E., Hu, T. X., Elder, K., Snell, P., Christie, L., Robson, P. and Niakan, K. K. (2015). Defining the three cell lineages of the human blastocyst by single-cell RNA-seq. *Development* **142**, 3151-3165. doi:10.1242/dev.123547
- Braam, S. R., Zeinstra, L., Litjens, S., Ward-van Oostwaard, D., van den Brink, S., van Laake, L., Lebrin, F., Kats, P., Hochstenbach, R., Passier, R. et al. (2008). Recombinant vitronectin is a functionally defined substrate that supports human embryonic stem cell self-renewal via  $\alpha$ 5 $\beta$ 1 integrin. *Stem Cells* **26**, 2257-2265. doi:10.1634/stemcells.2008-0291
- Cahan, P. and Daley, G. Q. (2013). Origins and implications of pluripotent stem cell variability and heterogeneity. *Nat. Rev. Mol. Cell Biol.* **14**, 357-368. doi:10.1038/nrm3584
- Chambers, I., Silva, J., Colby, D., Nichols, J., Nijmeijer, B., Robertson, M., Vrana, J., Jones, K., Grotewold, L. and Smith, A. (2007). Nanog safeguards pluripotency and mediates germline development. *Nature* **450**, 1230-1234. doi:10.1038/nature06403
- Chen, A. F., Liu, A. J., Krishnakumar, R., Freimer, J. W., DeVeale, B. and Belloch, R. (2018). GRHL2-dependent enhancer switching maintains a pluripotent stem cell transcriptional subnetwork after exit from naive pluripotency. *Cell Stem Cell* **23**, 226-238.e224. doi:10.1016/j.stem.2018.06.005
- Chuai, M., Zeng, W., Yang, X., Boychenko, V., Glazier, J. A. and Weijer, C. J. (2006). Cell movement during chick primitive streak formation. *Dev. Biol.* **296**, 137-149. doi:10.1016/j.ydbio.2006.04.451
- Chung, V. Y., Tan, T. Z., Tan, M., Wong, M. K., Kuay, K. T., Yang, Z., Ye, J., Muller, J., Koh, C. M., Guccione, E. et al. (2016). GRHL2-miR-200-ZEB1 maintains the epithelial status of ovarian cancer through transcriptional regulation and histone modification. *Sci. Rep.* **6**, 19943. doi:10.1038/srep19943

- Cieply, B., Riley, P. T., Pifer, P. M., Widmeyer, J., Addison, J. B., Ivanov, A. V., Denvir, J. and Frisch, S. M. (2012). Suppression of the epithelial-mesenchymal transition by Grainyhead-like-2. *Cancer Res.* **72**, 2440-2453. doi:10.1158/0008-5472.CAN-11-4038
- Deglincerti, A., Croft, G. F., Pietila, L. N., Zernicka-Goetz, M., Siggia, E. D. and Brivanlou, A. H. (2016a). Self-organization of the in vitro attached human embryo. *Nature* **533**, 251-254. doi:10.1038/nature17948
- Deglincerti, A., Etoc, F., Guerra, M. C., Martyn, I., Metzger, J., Ruzo, A., Simunovic, M., Yoney, A., Brivanlou, A. H., Siggia, E. et al. (2016b). Self-organization of human embryonic stem cells on micropatterns. *Nat. Protoc.* **11**, 2223-2232. doi:10.1038/nprot.2016.131
- Eyal-Giladi, H. and Kochav, S. (1976). From cleavage to primitive streak formation: a complementary normal table and a new look at the first stages of the development of the chick. I. General morphology. *Dev. Biol.* **49**, 321-337. doi:10.1016/0012-1606(76)90178-0
- Forristal, C. E., Wright, K. L., Hanley, N. A., Oreffo, R. O. and Houghton, F. D. (2010). Hypoxia inducible factors regulate pluripotency and proliferation in human embryonic stem cells cultured at reduced oxygen tensions. *Reproduction* **139**, 85-97. doi:10.1530/REP-09-0300
- Hamidi, S., Nakaya, Y., Nagai, H., Alev, C., Shibata, T. and Sheng, G. (2019). Biomechanical regulation of EMT and epithelial morphogenesis in amniote epiblast. *Phys. Biol.* **16**, 041002. doi:10.1088/1478-3975/ab1048
- Harrisson, F., Callebaut, M. and Vakaet, L. (1991). Features of polyingression and primitive streak ingression through the basal lamina in the chicken blastoderm. *Anat. Rec.* **229**, 369-383. doi:10.1002/ar.1092290310
- Hashimoto, M. and Sasaki, H. (2019). Epiblast formation by Tead-Yap-dependent expression of pluripotency factors and competitive elimination of unspecified cells. *Dev. Cell* **50**, 139-154. doi:10.1016/j.devcel.2019.05.024
- Hay, E. D. (1968). Organization and fine structure of epithelium and mesenchyme in the developing chick embryo. In *Epithelial-Mesenchymal Interactions; 18th Hahnemann Symposium* (ed. R. Fleischmajer and R. E. Billingham), pp. 31-55. Baltimore: Williams & Wilkins.
- Higuchi, S., Yoshina, S. and Mitani, S. (2016). Inhibition of the integrin signal constitutes a mouse iPS cell niche. *Dev. Growth Differ.* **58**, 586-599. doi:10.1111/dgd.12302
- Kallas, A., Pook, M., Maimets, M., Zimmermann, K. and Maimets, T. (2011). Nocodazole treatment decreases expression of pluripotency markers Nanog and Oct4 in human embryonic stem cells. *PLoS ONE* **6**, e19114. doi:10.1371/journal.pone.0019114
- Ke, M.-T., Nakai, Y., Fujimoto, S., Takayama, R., Yoshida, S., Kitajima, T. S., Sato, M. and Imai, T. (2016). Super-resolution mapping of neuronal circuitry with an index-optimized clearing agent. *Cell Rep.* **14**, 2718-2732. doi:10.1016/j.celrep.2016.02.057
- Kinoshita, M. and Smith, A. (2018). Pluripotency deconstructed. *Dev. Growth Differ.* **60**, 44-52. doi:10.1111/dgd.12419
- Kochav, S., Ginsburg, M. and Eyal-Giladi, H. (1980). From cleavage to primitive streak formation: a complementary normal table and a new look at the first stages of the development of the chick. II. Microscopic anatomy and cell population dynamics. *Dev. Biol.* **79**, 296-308. doi:10.1016/0012-1606(80)90117-7
- Lamouille, S., Xu, J. and Derynck, R. (2014). Molecular mechanisms of epithelial-mesenchymal transition. *Nat. Rev. Mol. Cell Biol.* **15**, 178-196. doi:10.1038/nrm3758
- Lavial, F., Aclouque, H., Bertocchini, F., MacLeod, D. J., Boast, S., Bachelard, E., Montillet, G., Thenot, S., Sang, H. M., Stern, C. D. et al. (2007). The Oct4 homologue PouV and Nanog regulate pluripotency in chicken embryonic stem cells. *Development* **134**, 3549-3563. doi:10.1242/dev.006569
- Lee, S., Ryu, J. H., Park, K., Lee, A., Lee, S.-Y., Youn, I.-C., Ahn, C.-H., Yoon, S. M., Myung, S.-J., Moon, D. H. et al. (2009). Polymeric nanoparticle-based activatable near-infrared nanosensor for protease determination in vivo. *Nano Lett.* **9**, 4412-4416. doi:10.1021/nl902709m
- Lei, Q.-Y., Zhang, H., Zhao, B., Zha, Z.-Y., Bai, F., Pei, X.-H., Zhao, S., Xiong, Y. and Guan, K.-L. (2008). TAZ promotes cell proliferation and epithelial-mesenchymal transition and is inhibited by the hippo pathway. *Mol. Cell Biol.* **28**, 2426-2436. doi:10.1128/MCB.01874-07
- Li, S., Qi, Y., McKee, K., Liu, J., Hsu, J. and Yurchenco, P. D. (2017). Integrin and dystroglycan compensate each other to mediate laminin-dependent basement membrane assembly and epiblast polarization. *Matrix Biol.* **57-58**, 272-284. doi:10.1016/j.matbio.2016.07.005
- Lizio, M., Deviatirov, R., Nagai, H., Galan, L., Arner, E., Itoh, M., Lassmann, T., Kasukawa, T., Hasegawa, A., Ros, M. A. et al. (2017). Systematic analysis of transcription start sites in avian development. *PLoS Biol.* **15**, e2002887. doi:10.1371/journal.pbio.2002887
- Luckett, W. P. (1975). The development of primordial and definitive amniotic cavities in early Rhesus monkey and human embryos. *Am. J. Anat.* **144**, 149-167. doi:10.1002/aja.1001440204
- Luckett, W. P. (1978). Origin and differentiation of the yolk sac and extraembryonic mesoderm in presomite human and rhesus monkey embryos. *Am. J. Anat.* **152**, 59-97. doi:10.1002/aja.1001520106
- Mak, S. S., Alev, C., Nagai, H., Wrabel, A., Matsuoka, Y., Honda, A., Sheng, G. and Ladher, R. K. (2015). Characterization of the finch embryo supports evolutionary conservation of the naive stage of development in amniotes. *Elife* **4**, e07178. doi:10.7554/eLife.07178.012
- Martinez-Rico, C., Pincet, F., Thiery, J.-P. and Dufour, S. (2010). Integrins stimulate E-cadherin-mediated intercellular adhesion by regulating Src-kinase activation and actomyosin contractility. *J. Cell Sci.* **123**, 712-722. doi:10.1242/jcs.047878
- Masuda-Hirata, M., Suzuki, A., Amano, Y., Yamashita, K., Ide, M., Yamanaka, T., Sakai, M., Imamura, M. and Ohno, S. (2009). Intracellular polarity protein PAR-1 regulates extracellular laminin assembly by regulating the dystroglycan complex. *Genes Cells* **14**, 835-850. doi:10.1111/j.1365-2443.2009.01315.x
- Mathew, B., Muñoz-Descalzo, S., Corujo-Simón, E., Schroter, C., Stelzer, E. H. K. and Fischer, S. C. (2019). Mouse ICM organoids reveal three-dimensional cell fate clustering. *Biophys. J.* **116**, 127-141. doi:10.1016/j.bpj.2018.11.011
- Mathieu, J., Zhang, Z., Nelson, A., Lamba, D. A., Reh, T. A., Ware, C. and Ruohola-Baker, H. (2013). Hypoxia induces re-entry of committed cells into pluripotency. *Stem Cells* **31**, 1737-1748. doi:10.1002/stem.1446
- Mooney, S. M., Talebian, V., Jolly, M. K., Jia, D., Gromala, M., Levine, H. and McConkey, B. J. (2017). The GRHL2/ZEB feedback loop-a key axis in the regulation of EMT in breast cancer. *J. Cell. Biochem.* **118**, 2559-2570. doi:10.1002/jcb.25974
- Morgani, S. M., Metzger, J. J., Nichols, J., Siggia, E. D. and Hadjantonakis, A. K. (2018). Micropattern differentiation of mouse pluripotent stem cells recapitulates embryo regionalized cell fate patterning. *Elife* **7**, e32839. doi:10.7554/eLife.32839.029
- Mui, K. L., Chen, C. S. and Assoian, R. K. (2016). The mechanical regulation of integrin-cadherin crosstalk organizes cells, signaling and forces. *J. Cell Sci.* **129**, 1093-1100. doi:10.1242/jcs.183699
- Najm, F. J., Chenoweth, J. G., Anderson, P. D., Nadeau, J. H., Redline, R. W., McKay, R. D. G. and Tesar, P. J. (2011). Isolation of epiblast stem cells from preimplantation mouse embryos. *Cell Stem Cell* **8**, 318-325. doi:10.1016/j.stem.2011.01.016
- Nakamura, T., Okamoto, I., Sasaki, K., Yabuta, Y., Iwatani, C., Tsuchiya, H., Seita, Y., Nakamura, S., Yamamoto, T. and Saitou, M. (2016). A developmental coordinate of pluripotency among mice, monkeys and humans. *Nature* **537**, 57-62. doi:10.1038/nature19096
- Nakanishi, M., Mitchell, R. R., Benoit, Y. D., Orlando, L., Reid, J. C., Shimada, K., Davidson, K. C., Shapovalova, Z., Collins, T. J., Nagy, A. et al. (2019). Human pluripotency is initiated and preserved by a unique subset of founder cells. *Cell* **177**, 910-924. doi:10.1016/j.cell.2019.03.013
- Nakanoh, S., Fuse, N., Takahashi, Y. and Agata, K. (2015). Verification of chicken Nanog as an epiblast marker and identification of chicken PouV as Pou5f3 by newly raised antibodies. *Dev. Growth Differ.* **57**, 251-263. doi:10.1111/dgd.12205
- Nakaya, Y. and Sheng, G. (2008). Epithelial to mesenchymal transition during gastrulation: an embryological view. *Dev. Growth Differ.* **50**, 755-766. doi:10.1111/j.1440-169X.2008.01070.x
- Nakaya, Y., Sukowati, E. W., Wu, Y. and Sheng, G. (2008). RhoA and microtubule dynamics control cell-basement membrane interaction in EMT during gastrulation. *Nat. Cell Biol.* **10**, 765-775. doi:10.1038/ncb1739
- Nakaya, Y., Sukowati, E. W., Alev, C., Nakazawa, F. and Sheng, G. (2011). Involvement of dystroglycan in epithelial-mesenchymal transition during chick gastrulation. *Cells Tissues Organs* **193**, 64-73. doi:10.1159/000320165
- Nakaya, Y., Sukowati, E. W. and Sheng, G. (2013). Epiblast integrity requires CLASP and Dystroglycan-mediated microtubule anchoring to the basal cortex. *J. Cell Biol.* **202**, 637-651. doi:10.1083/jcb.201302075
- Nakazawa, F., Nagai, H., Shin, M. and Sheng, G. (2006). Negative regulation of primitive hematopoiesis by the FGF signaling pathway. *Blood* **108**, 3335-3343. doi:10.1182/blood-2006-05-021386
- Narsinh, K. H., Sun, N., Sanchez-Freire, V., Lee, A. S., Almeida, P., Hu, S., Jan, T., Wilson, K. D., Leong, D., Rosenberg, J. et al. (2011). Single cell transcriptional profiling reveals heterogeneity of human induced pluripotent stem cells. *J. Clin. Invest.* **121**, 1217-1221. doi:10.1172/JCI44635
- Nichols, J. and Smith, A. (2009). Naive and primed pluripotent states. *Cell Stem Cell* **4**, 487-492. doi:10.1016/j.stem.2009.05.015
- Nieto, M. A., Huang, R. Y.-J., Jackson, R. A. and Thiery, J. P. (2016). EMT: 2016. *Cell* **166**, 21-45. doi:10.1016/j.cell.2016.06.028
- Niwa, H., Nakamura, A., Urata, M., Shirae-Kurabayashi, M., Kuraku, S., Russell, S. and Ohtsuka, S. (2016). The evolutionarily-conserved function of group B1 Sox family members confers the unique role of Sox2 in mouse ES cells. *BMC Evol. Biol.* **16**, 173. doi:10.1186/s12862-016-0755-4
- Plouffe, S. W., Lin, K. C., Moore, J. L., III, Tan, F. E., Ma, S., Ye, Z., Qiu, Y., Ren, B. and Guan, K.-L. (2018). The Hippo pathway effector proteins YAP and TAZ have both distinct and overlapping functions in the cell. *J. Biol. Chem.* **293**, 11230-11240. doi:10.1074/jbc.RA118.002715
- Qin, H., Hejna, M., Liu, Y., Percharde, M., Wossidlo, M., Blouin, L., Durruthy-Durruthy, J., Wong, P., Qi, Z., Yu, J. et al. (2016). YAP induces human naive pluripotency. *Cell Rep.* **14**, 2301-2312. doi:10.1016/j.celrep.2016.02.036
- Robles, V., Marti, M. and Belmonte, J. C. I. (2011). Study of pluripotency markers in zebrafish embryos and transient embryonic stem cell cultures. *Zebrafish* **8**, 57-63. doi:10.1089/zeb.2010.0684

- Rodin, S., Domogatskaya, A., Ström, S., Hansson, E. M., Chien, K. R., Inzunza, J., Hovatta, O. and Tryggvason, K. (2010). Long-term self-renewal of human pluripotent stem cells on human recombinant laminin-511. *Nat. Biotechnol.* **28**, 611-615. doi:10.1038/nbt.1620
- Rosselló, R. A., Chen, C.-C., Dai, R., Howard, J. T., Hochgeschwender, U. and Jarvis, E. D. (2013). Mammalian genes induce partially reprogrammed pluripotent stem cells in non-mammalian vertebrate and invertebrate species. *Elife* **2**, e00036. doi:10.7554/eLife.00036
- Sakai, T., Li, S., Docheva, D., Grashoff, C., Sakai, K., Kostka, G., Braun, A., Pfeifer, A., Yurchenco, P. D. and Fassler, R. (2003). Integrin-linked kinase (ILK) is required for polarizing the epiblast, cell adhesion, and controlling actin accumulation. *Genes Dev.* **17**, 926-940. doi:10.1101/gad.255603
- Schnerch, A., Cerdan, C. and Bhatia, M. (2010). Distinguishing between mouse and human pluripotent stem cell regulation: the best laid plans of mice and men. *Stem Cells* **28**, 419-430. doi:10.1002/stem.298
- Shahbazi, M. N., Scialdone, A., Skorupska, N., Weberling, A., Recher, G., Zhu, M., Jedrusik, A., Devito, L. G., Noli, L., Macaulay, I. C. et al. (2017). Pluripotent state transitions coordinate morphogenesis in mouse and human embryos. *Nature* **552**, 239-243. doi:10.1038/nature24675
- Sharma, S., Lee, A., Choi, K., Kim, K., Youn, I., Trippel, S. B. and Panitch, A. (2013). Biomimetic aggrecan reduces cartilage extracellular matrix from degradation and lowers catabolic activity in ex vivo and in vivo models. *Macromol. Biosci.* **13**, 1228-1237. doi:10.1002/mabi.201300112
- Sheng, G. (2015). Epiblast morphogenesis before gastrulation. *Dev. Biol.* **401**, 17-24. doi:10.1016/j.ydbio.2014.10.003
- Shimaoka, M., Takagi, J. and Springer, T. A. (2002). Conformational regulation of integrin structure and function. *Annu. Rev. Biophys. Biomol. Struct.* **31**, 485-516. doi:10.1146/annurev.biophys.31.101101.140922
- Shin, M., Alev, C., Wu, Y., Nagai, H. and Sheng, G. (2011). Activin/TGF-beta signaling regulates Nanog expression in the epiblast during gastrulation. *Mech. Dev.* **128**, 268-278. doi:10.1016/j.mod.2011.03.001
- Siliciano, J. D. and Goodenough, D. A. (1988). Localization of the tight junction protein, ZO-1, is modulated by extracellular calcium and cell-cell contact in Madin-Darby canine kidney epithelial cells. *J. Cell Biol.* **107**, 2389-2399. doi:10.1083/jcb.107.6.2389
- Stemmler, M. P., Eccles, R. L., Brabletz, S. and Brabletz, T. (2019). Non-redundant functions of EMT transcription factors. *Nat. Cell Biol.* **21**, 102-112. doi:10.1038/s41556-018-0196-y
- Stern, C. D. and Downs, K. M. (2012). The hypoblast (visceral endoderm): an evo-devo perspective. *Development* **139**, 1059-1069. doi:10.1242/dev.070730
- Stumpf, P. S., Smith, R. C. G., Lenz, M., Schuppert, A., Muller, F. J., Babbie, A., Chan, T. E., Stumpf, M. P. H., Please, C. P., Howison, S. D. et al. (2017). Stem cell differentiation as a non-markov stochastic process. *Cell Syst.* **5**, 268-282.e267. doi:10.1016/j.cels.2017.08.009
- Takahashi, K., Tanabe, K., Ohnuki, M., Narita, M., Ichisaka, T., Tomoda, K. and Yamanaka, S. (2007). Induction of pluripotent stem cells from adult human fibroblasts by defined factors. *Cell* **131**, 861-872. doi:10.1016/j.cell.2007.11.019
- Tesar, P. J., Chenoweth, J. G., Brook, F. A., Davies, T. J., Evans, E. P., Mack, D. L., Gardner, R. L. and McKay, R. D. G. (2007). New cell lines from mouse epiblast share defining features with human embryonic stem cells. *Nature* **448**, 196-199. doi:10.1038/nature05972
- Villa-Diaz, L. G., Kim, J. K., Laperle, A., Palecek, S. P. and Krebsbach, P. H. (2016). Inhibition of focal adhesion kinase signaling by integrin  $\alpha 6 \beta 1$  supports human pluripotent stem cell self-renewal. *Stem Cells* **34**, 1753-1764. doi:10.1002/stem.2349
- Vitillo, L., Baxter, M., Iskender, B., Whiting, P. and Kimber, S. J. (2016). Integrin-associated focal adhesion kinase protects human embryonic stem cells from apoptosis, detachment, and differentiation. *Stem Cell Reports* **7**, 167-176. doi:10.1016/j.stemcr.2016.07.006
- Vogler, H. (1987). Human blastogenesis. Formation of the extraembryonic cavities. *Bibl. Anat.* **30**, 1-148.
- Voiculescu, O., Bertocchini, F., Wolpert, L., Keller, R. E. and Stern, C. D. (2007). The amniote primitive streak is defined by epithelial cell intercalation before gastrulation. *Nature* **449**, 1049-1052. doi:10.1038/nature06211
- Waddington, C. H. (1952). *The Epigenetics of Birds*. Cambridge Eng: University Press.
- Warmflash, A., Sorre, B., Etoc, F., Siggia, E. D. and Brivanlou, A. H. (2014). A method to recapitulate early embryonic spatial patterning in human embryonic stem cells. *Nat. Methods* **11**, 847-854. doi:10.1038/nmeth.3016
- Watanabe, K., Ueno, M., Kamiya, D., Nishiyama, A., Matsumura, M., Wataya, T., Takahashi, J. B., Nishikawa, S., Nishikawa, S., Muguruma, K. et al. (2007). A ROCK inhibitor permits survival of dissociated human embryonic stem cells. *Nat. Biotechnol.* **25**, 681-686. doi:10.1038/nbt1310
- Weinberger, C. and Brick, I. (1982). Primary hypoblast development in the chick: I. Scanning electron microscopy of normal development. *Wilhelm Roux Arch. Dev. Biol.* **191**, 119-126. doi:10.1007/BF00848449
- Weinberger, L., Ayyash, M., Novershtern, N. and Hanna, J. H. (2016). Dynamic stem cell states: naive to primed pluripotency in rodents and humans. *Nat. Rev. Mol. Cell Biol.* **17**, 155-169. doi:10.1038/nrm.2015.28
- Woichansky, I., Beretta, C. A., Berns, N. and Riechmann, V. (2016). Three mechanisms control E-cadherin localization to the zonula adherens. *Nat. Commun.* **7**, 10834. doi:10.1038/ncomms10834
- Wu, W.-S., You, R.-I., Cheng, C.-C., Lee, M.-C., Lin, T.-Y. and Hu, C.-T. (2017). Snail collaborates with EGR-1 and SP-1 to directly activate transcription of MMP 9 and ZEB1. *Sci. Rep.* **7**, 17753. doi:10.1038/s41598-017-18101-7
- Xiao, H., Jiang, N., Zhou, B., Liu, Q. and Du, C. (2015). TAZ regulates cell proliferation and epithelial-mesenchymal transition of human hepatocellular carcinoma. *Cancer Sci.* **106**, 151-159. doi:10.1111/cas.12587
- Yagi, T., Ito, D., Okada, Y., Akamatsu, W., Nihei, Y., Yoshizaki, T., Yamanaka, S., Okano, H. and Suzuki, N. (2011). Modeling familial Alzheimer's disease with induced pluripotent stem cells. *Hum. Mol. Genet.* **20**, 4530-4539. doi:10.1093/hmg/ddr394
- Zhou, X., Chadarevian, J. P., Ruiz, B. and Ying, Q.-L. (2017). Cytoplasmic and nuclear TAZ exert distinct functions in regulating primed pluripotency. *Stem Cell Reports* **9**, 732-741. doi:10.1016/j.stemcr.2017.07.019

**SUPPLEMENTARY FIGURES AND TABLES**

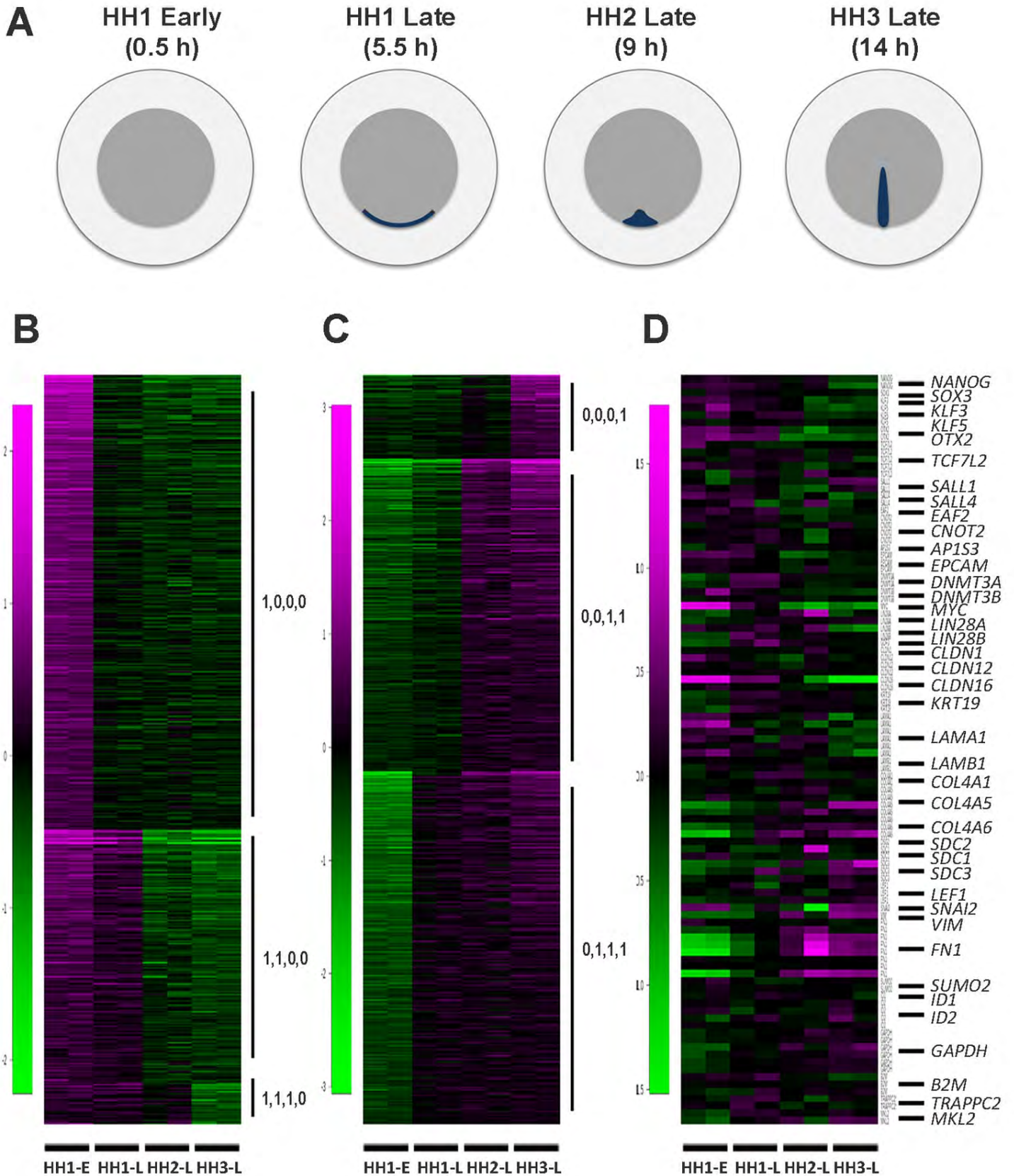


**Figure S1: Transcriptomic analysis of pre-gastrulation chicken epiblast.** (A) Schematic representation of epiblast tissues used for the analysis. HH1 early: 0.5 hour of incubation; HH1 late: 5.5 hours; HH2 late: 9 hours; HH3 late: 14 hours. Only dark grey areas were collected for Affymetrix chicken genechip analysis. (B-D) Clustering analysis of cross-stage variations, showing significantly down-regulated genes (B), significantly upregulated genes (C) and genes associated with pluripotency regulation and epithelial morphogenesis (D). Each stage is represented by duplicate samples.

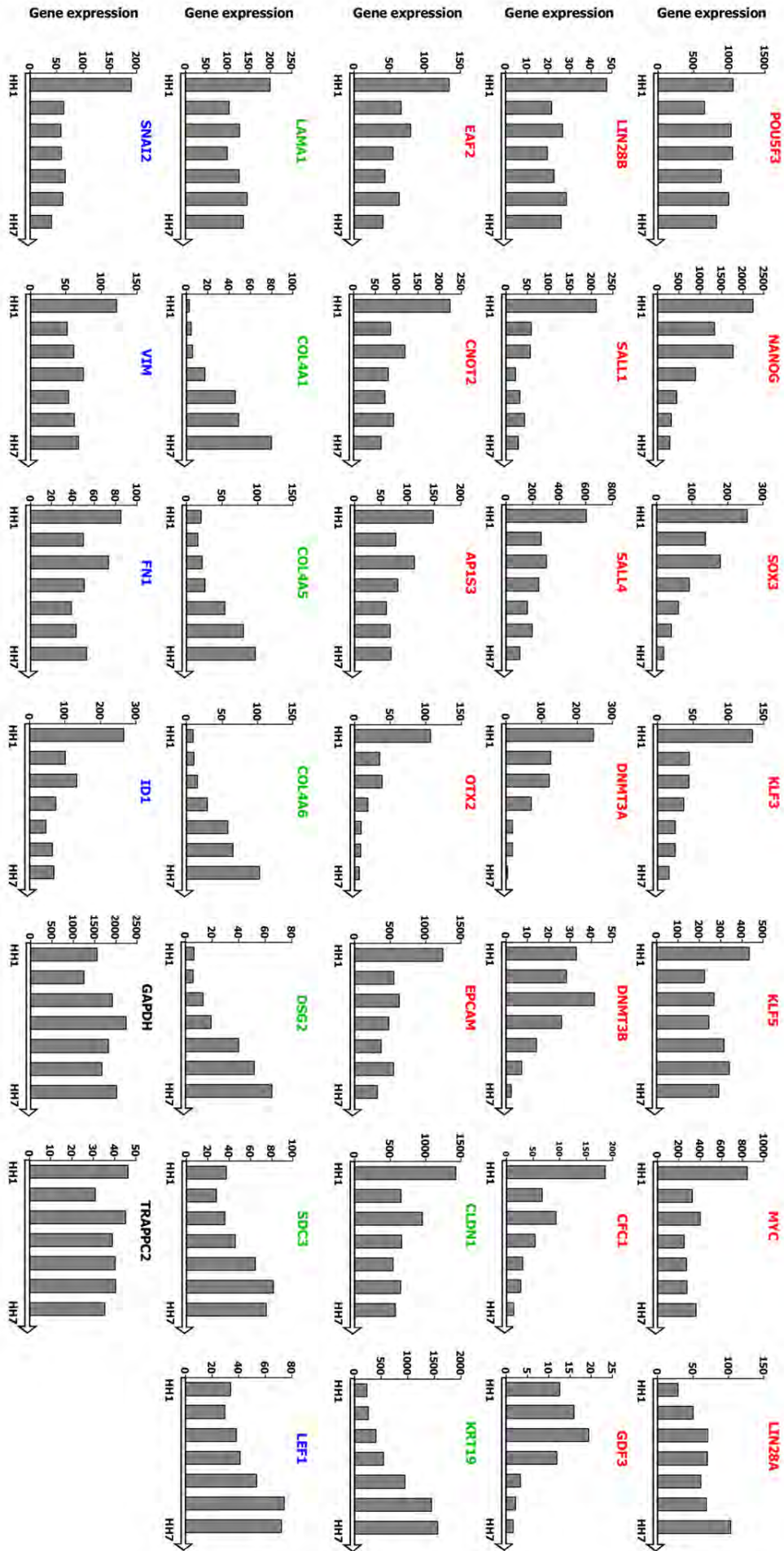


**Figure S2: CAGE-based promoter activity of selected genes in early chicken development, from HH1 to HH7.** Raw values were extracted from the chicken ZENBU database. Gene names are listed above each panel. Red: pluripotency-related genes; Green: genes related to epithelial features; Blue: genes related to mesenchymal features; Black: housekeeping genes.



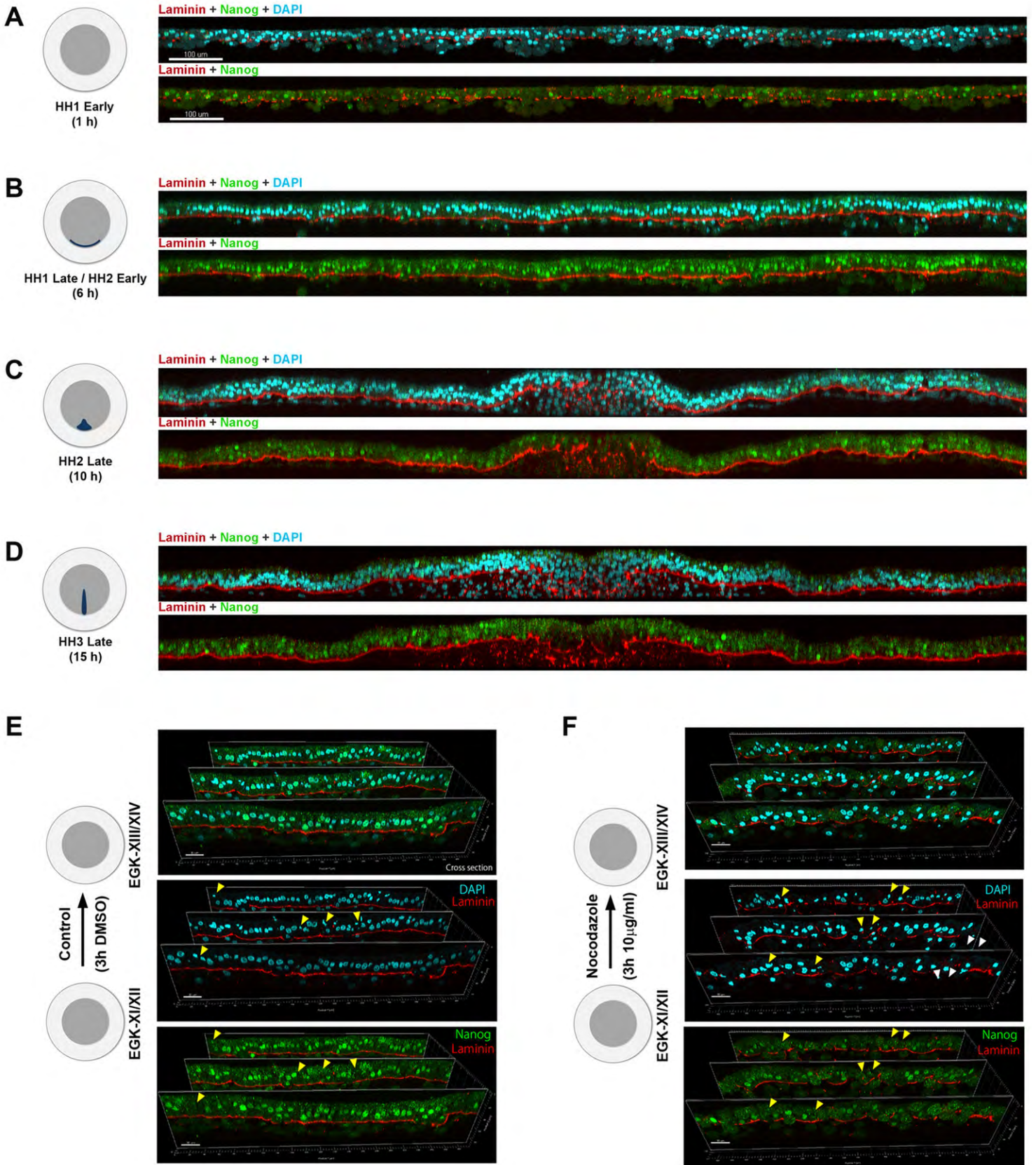
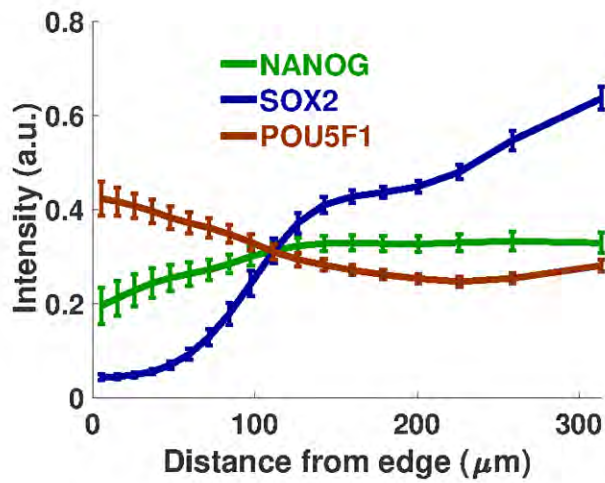


**Figure S4: Partial MET during avian epiblast morphogenesis correlates with a progressive pluripotency loss.** (A-D) Representative confocal images of embryo sections stained for Laminin (red) and NANOG (green). A: early HH1 (1 hour of incubation); B: late HH1/early HH2 (6 hours); C: late HH2 (10 hours); D: late HH3 (15 hours). In panels C and D, gastrulation EMT is visible in the primitive streak. Scale bar in A-D: 100  $\mu\text{m}$ . (E,F) Control and nocodazole treated embryos stained for NANOG and Laminin. (E): Embryos were pre-incubated for 4 hours under normal conditions and then treated with control (DMSO) for 3 hours. Epiblast cells express NANOG robustly in all control epiblast cells (except in dividing cells, arrowheads). (F): Embryos were pre-incubated for 4 hours under normal conditions and then treated with nocodazole for 3 hours. Nocodazole treatment resulted in Laminin (red) breakdown and in a reduction of NANOG (green) expression level. Nocodazole treatment lowers NANOG nuclear expression (with some examples indicated by arrowheads). Scale bar in E, F: 20  $\mu\text{m}$ .

**A**



**B**

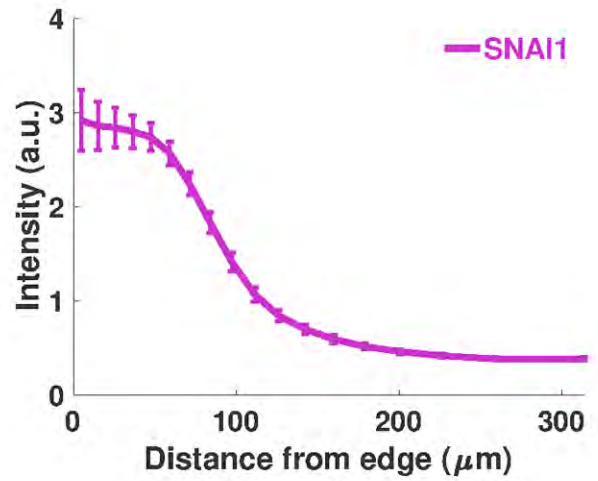


**Figure S5: BMP-induced differentiation of micropatterned hESCs.** (A) Both NANOG and POU5F1 show strong decrease upon BMP-induced differentiation (compared with expression levels shown in Fig.7B). In contrast, SOX2 shows an increase in colony center upon BMP treatment, marking neuroectoderm lineage differentiation. (B) SNAI1 shows dramatic increase in colony pericenter, after BMP treatment, marking mesendoderm differentiation.

**Table S1: Chicken epiblast Affymetrix genechip data.**

[Click here to Download Table S1](#)

**Table S2: Gene ontology analysis of significantly changed epiblast genes from HH1 to HH3.**

[Click here to Download Table S2](#)

**Table S3: Expression levels of Integrin genes obtained from promoterome and transcriptome analyses.**

CAGE-based promoter activity data for chicken samples are based on Lizio et al, 2017. Chicken transcriptome data are based on Affymetrix dataset presented in this work. CAGE-based promoter activity data for human iPSCs are based on (Arner et al., 2015) and human transcriptome data are based on Affymetrix dataset presented in (Yagi et al., 2011).

[Click here to Download Table S3](#)